due to clinical signs of infection/inflammation, 18 samples (14%) were submitted to rule out intraocular lymphoma, 9 fluids for reasons like intravitreal foreign bodies or vitreous opacities, 9 samples for intraocular hemorrhage (7%), 6 fluids to rule out amyloidosis (4%), 4 to rule out melanoma (3%), and in 7 samples (5%) no clinical history was provided. The amount of fluid received varied from 0.5 – 150 cc and cytospins and Thin Preps were the methods of preparation used. Fluids displayed few patterns: paucicellular (37%), mixed chronic inflammation (36%), acute inflammation (17%), malignant (4%) and hemorrhage (4.5%). GMS stain performed in 56% of fluids where infection was suspected showed presence of fungal hyphae in 4 cases. No viral inclusions were seen (in 2 cases PCR for herpes simplex and CMV viruses was negative) and one fluid showed present Gram positive cocci on Gram stain performed. Flow cytometry studies were attempted in 72% of cases where intraocular lymphoma was in the differential diagnosis; 5 of them had insufficient cellularity or were technically suboptimal, 7 were negative for a B-cell proliferation and 1 was positive. In 2 cases immunohistochemical stains were performed on smears or concomitant biopsy. Two cases showed high grade lymphoma (1.5%), one large cell B-cell type, one high grade T-cell type, natural killer phenotype. Three cases (2%) were positive for malignant melanoma and abundant amyloid deposition was found in 1 case by Congo Red stain.
Conclusions: Cytologic analysis of vitreous fluid is very useful in evaluation of ocular pathology. The addition of special stains and modern techniques like flow cytometry or PCR, further expands the diagnostic possibilities.

Pathobiology

1654 Targeted Disruption of the CSF-1 Gene Leads to Osteopetrosis and Osteoblast Defects .

S Abboud Werner, D Horn, K Woodruff, R Fajardo, M Harris, S Harris. University of Texas Health Science Center, San Antonio.
Background: CSF-1, a key determinant of osteoclast-mediated bone remodeling, is highly expressed by osteoblasts and osteocytes. CSF-1 deficiency in spontaneous mutant op/op mice decreases macrophages/osteoclasts and leads to osteopetrosis and a pleiotropic phenotype. The effect of CSF-1 knockout (KO) in all tissues or conditional KO of CSF-1 using a Cre/loxP system has not been explored. Objective: To determine the effect of inactivation of CSF-1 and develop a strategy for examining the biologic effect of CSF-1 KO in bone using Cre-lox technology.
Design: A targeting vector for generating a conditional KO allele for CSF-1 (deleting exons 4,5,6) was used to generate heterozygous mice harboring the floxed construct without a neo cassette (fx allele). CSF-1fx/CSF-1fx mice were bred with Meox2Cre mice to produce mice homozygous for the KO allele(hCSF-1KO). (Meox2 promoter drives expression of Cre throughout the epiblast). At 3 weeks, hCSF-1KO and WT littermates were analyzed for CSF-1 protein and F4/80+ macrophages. Hind limbs were examined by x-ray, microCT, histology and stained with TRAP and CD31 to identify osteoclasts and vessels, respectively.
Results: Homozygous (h)CSF-1KO showed absence of CSF-1 in all tissues, reduced macrophages in most organs, decreased circulating monocytes and osteopetrosis with failure of tooth eruption similar to op/op mice. Radiographs of hCSF-1KO showed marked skeletal sclerosis and, by microCT, %BV/TV and trabecular number were increased and cortical bone thickness was decreased; bone mineral density was increased by DEXA scan. Histologically, hCSF-1KO bones showed an expanded growth plate, increased bone trabeculae with prominent cartilage cores replacing the marrow cavity, narrow vascular sinusoids and poorly formed cortical bone. Numerous TRAP+ osteoclasts were identified in WT, whereas rare mononucleated osteoclast-like cells were detected in CSF-1KO bone. In CSF-1KO, osteoblasts showed loss of polarity; matrix formation and collagen fibrils were disorganized and abnormal clusters of osteocytes entrapped in matrix were identified.
Conclusions: Results provide the first evidence that global CSF-1KO using a Meox2Cre-based system leads to osteopetrosis and alters osteoblast function. Conditional KO of CSF-1 in bone cells is feasible and will be crucial for elucidating the mechanisms by which CSF-1 exerts pleiotropic effects and regulates bone turnover and repair.

1655 Immunophenotypic Characterization of Epithelial-Stromal Interface Cells.

P Adegboyega. LSU Health Sciences Center, Shreveport.
Background: In visceral organs, the epithelium and the stroma are separated by a layer of stromal cells and the basement membrane. These epithelial-stromal interface (ESI) cells are known to play significant regulatory roles in the organogenesis, differentiation and homeostasis of the overlying epithelium. In the gastrointestinal tract as well as in other viscera, these cells are also postulated to play critical roles in inflammation, restitution, and regeneration of damaged epithelium and also involved in neoplastic transformation and proliferation of the epithelial cells in the process of carcinogenesis and tumorigenesis respectively. However, the histogenesis and the biology of these cells are yet to be elucidated. Hence this study, to characterize the immunophenotypic features of these cells in skin adnexae and visceral organs.
Design: Benign samples were obtained from resection specimens of the following organs: Skin (n=10), breast (n=10), parotid gland (n=10), pancreas (n=10), prostate (n=10), small bowel (n=10) and colon (n=15). The tissue samples were fixed in formalin solution and paraffin-embedded for routine H&E. Representative sections were immunostained for the followings: 5 cytokeratins that are reportedly expressed in myoepithelial cells (CK5, CK7, CK8, CK14, CK18, CK19 and K903), 6 non-keratin related structure-specific microfilaments and intermediate filaments (alpha smooth muscle [SMA], calponin, desmin, H-caldesmon, smooth muscle myosin heavy chain [SMMHC], and vimentin) and 7 nonstructural proteins (CD10, CD34, CD117, GFAP, maspin, p63, and S100). Immunohistochemistry was done using avidin-biotin detection method with antigen retrieval.
Results: ESIs in both small and large intestinal mucosa expressed smooth muscle–related microfilaments and intermediate filaments ([SMA, calponin, H-caldesmon, SMMHC) and vimentin; but stained negative with desmin, all the cytokeratins and the nonstructural proteins.
Conclusions: ESIs in the small and large bowel have similar immunophenotypic features; but in their lack of expression of the keratins and the non structural proteins studied, are distinctly different from the corresponding (myoepithelial) cells in other glandular organs such as breast, prostate and skin adnexal structures where they have been proposed to be the progenitor cells for the epithelium. Our results also show that the immunophenotypic features and the biology of the interface subepithelial stromal cells appear to vary from organ to organ. Therefore, reports of observations of such cells in one organ may not necessarily be true for the counterpart cells in another organ.

1656 Anatomic Study of the Renal Sympathetic Nervous System.

DS Atherton, FO Mendelsohn. Princeton Medical Center, Birmingham, AL.
Background: Hypertension affects millions of patients worldwide causing an enormous disease burden. Despite extensive pharmacologic therapy, the contribution of hypertension to death, stroke, myocardial infarction, and congestive heart failure remains significant. Despite these many pharmacologic therapies, blood pressure control remains suboptimal. This has prompted novel device therapies for blood pressure control. A renal nerve ablation catheter has been developed that can destroy the innervation of the kidneys using radiofrequency energy, which has been associated with significant decreases in blood pressure. The anatomic substrate for this device has been poorly described even though the therapy holds great promise. We report the first detailed anatomic study of the renovascular wall and nervous system in renal arteries studied at autopsy.
Design: Left and right renal arteries (n=6) were obtained at autopsy from patients who died at our institution from natural causes. Unusual anatomic variants and arteries that demonstrated significant atherosclerosis or other structural compromise due to underlying pathology were excluded. Representative proximal, middle, and distal cross sections were obtained from each artery. The distance of peripheral nerves within the adventitia and surrounding soft tissue were measured relative to the lumen using an Olympus ocular micrometer.
Results: The distance from the lumen to closest nerve assessed was 0.4mm and the distance from the lumen to the farthest nerve assessed was 3.1mm. The average percentage of total nerves existing at increasing intervals from the artery lumen was 43.3±10.4% from 0.4-1.0mm, 28.5±8.3% from 1.0-1.5mm, 14.3±3.7% from 1.5-2.0mm, 7.99±2.3% from 2.0-2.5mm, and 5.80±3.3% at >2.5mm.
Conclusions: Our data shows that individual nerve fibers are more prevalent at closer intervals to the renal artery lumen, which could be due to increasing segmentation of peripheral nerves as they travel into and through the adventitia. If radiofrequency energy is sufficient to ablate nerves up to 1.5mm from the lumen, approximately 70% of nerves within 3mm will likely be affected. Likewise, if radiofrequency energy is sufficient to ablate nerves up to 2.5mm from the lumen, approximately 95% of nerves will be affected. This could suggest that relatively conservative radiofrequency energies could be used to still ablate a significant proportion of nerves.

1657 Development of a Scoring System for PTEN Immunohistochemistry in Breast Cancer.

R Bakkar, D Urbauer, R Broaddus. MD Anderson Cancer Center, Houston, TX.
Background: Loss of expression of PTEN, which inhibits the PI3K pathway, occurs in many types of cancer, including breast cancer. Patients with PTEN-deficient cancers may potentially benefit from PI3K pathway inhibitors, which are rapidly being developed and tested clinically. In breast cancer, loss of PTEN expression is associated with resistance to anti-hormonal therapy and Herceptin. Therefore, accurate identification of the subsets of breast cancer patients with PTEN loss is clinically important. Currently, there is no standardized protocol for pathological reporting of PTEN immunohistochemical results in breast cancer. Therefore, we wanted to design a practical scoring system with reliable clinical implications on patient outcome.
Design: Forty formalin fixed paraffin embedded breast carcinomas were immunohistochemically stained for PTEN using the Dako 6H2.1 antibody. Immunohistochemistry for anti-phosphorylated (serine 235/236) S6 ribosomal protein (pS6), a downstream member of the PI3K pathway, was scored as % positive. Cochran-Armitage trend and Fischer's exact tests were used for statistical analyses. The breast cancer results were compared to those from our previous study of 154 endometrial carcinomas.
Results: A 3-tiered scoring system (negative, reduced, positive) was devised. In all cases, the stroma stained strongly positive for PTEN. Positive was defined as tumor PTEN expression comparable to stroma PTEN expression. Negative was defined as a tumor with complete lack of PTEN. Reduced was defined as a tumor with less PTEN expression compared to internal control stroma. Significantly elevated pS6 expression in the negative tumors helped to validate this scoring system. Positive PTEN was present in 27.5% of cases; this correlated with ER positivity (p=0.009) and the absence of the triple negative subtype (p=0.04). The expression pattern of PTEN in the in situ component tended to reflect that of the invasive component. Interestingly, the reduced PTEN category is not identified in endometrial carcinoma.
Conclusions: Positive PTEN expression in breast cancer is associated with ER expression and the lack of the triple negative subtype, factors indicative of a better clinical outcome. The accuracy of our 3-tiered scoring system relies, in part, on careful comparison of tumor PTEN expression to stromal PTEN expression. The pattern of

PTEN expression in breast carcinoma is distinct from that we have previously reported in a large study of endometrial carcinoma. This suggests that it may be necessary to devise unique PTEN scoring systems for cancers derived from different organ systems.

1658 Modeling Neurogenetic Disorders Via Induced Pluripotent Stem Cells – A Novel Alternative for Pathology.

Y Bao, AJ Huttner. Yale University School of Medicine, New Haven, CT.

Background: Recent progress in our understanding of somatic cell reprogramming, particularly the isolation and characterization of human induced pluripotent stem cells (iPSCs) opened new avenues for modeling human disease. IPSCs allow the generation of large numbers of genetically modifiable cells specific to the underlying human genetic background, and form an unparalleled opportunity to gain new insight into disease pathophysiology. This will further lay the foundation for the development of patient specific pharmacological assays and/or stem cell based therapies. We focused on Walker Warburg Syndrome (WWS), a rare and severe form of congenital muscular dystrophy associated with lissencephaly. Most children die before the age of three years. Several genes have been implicated in the etiology of this syndrome, however, to this date the pathogenesis is poorly understood. In addition, none of the animal models appears to faithfully reflect the human condition. Patient derived IPSCs, however, allow the targeted differentiation of cells into tissue specific phenotypes of brain and muscle, and thus provide an assay for the recapitulation of disease specific pathophysiology.

Design: IPSC lines were derived from skin biopsy specimens of patients with WWS and normal age matched controls. We have achieved reprogramming of human fibroblasts using a lentiviral construct expressing human OCT4, SOX2, KLF4 and c-Myc/mCherry. The cells were grown in culture and differentiated into neurons, astrocytes and/or muscle. The in vivo potential of these progenitor cells was tested via in utero transplantation, which demonstrates the cells' ability to follow microenvironmental cues, migrate and differentiate appropriately.

Results: Directed differentiation of iPSCs into neuronal and myogenic precursors was demonstrated in vitro with antibodies for CNS phenotypes, like GFAP, TUJ1, Tbr1/2 as well as muscle phenotypes. The engraftment and integration of individual cells in vivo showed the ability of iPSCs to differentiate appropriately and show a disease specific difference to their normal counterpart.

Conclusions: This model allows the phenotypic recapitulation of complex neurogenetic traits, and provides insights into the pathophysiology of human forms of WWS.

1659 Androgen and Notch Signaling Gene Signatures Are Associated with Progression in Superfically Invasive Urothelial Carcinomas.

DM Berman, B William, S Luciana, R Ashley, F Jinshui, C Christopher, N Georges, S Edward, M Luigi, M Per-Uno. Johns Hopkins University, Baltimore, MD; Uppsala University, Sweden.

Background: Androgen receptor (AR) and Notch signaling may mediate aspects of urothelial carcinoma (UroCa) progression and thus serve as useful biomarkers for titrating therapy. UroCa occurs far more often in males, and AR signaling is required for bladder cancer formation and growth. Notch signaling maintains stem cells and regulates cell fate in development and cancer.

Design: We comprehensively profiled gene expression from cancer cells laser-captured from formalin-fixed paraffin-embedded (FFPE) bladder biopsies from 38 patients with pT UroCa. 19 patients progressed (Prog; median 22 mos) and 19 did not (NProg; median follow-up 84 mos). 14 received intravesical therapy (mitomycin C or BCG) after sampling. FFPE blocks were stored 8 to 26 years prior to sectioning. 22,000 gene profiling used the cDNA-mediated Annealing, Selection, Extension, and Ligation (DASL) system (Illumina, San Diego, CA). Bioinformatic analyses used R/Bioconductor. After quantile normalization, moderated t statistics and adjusted p values were obtained after fitting a linear model that accounted for progression and intravescical treatment effects. Functional themes were obtained from www.NetPath.org. Enrichment analysis was performed by ranking genes by their t-statistics, and testing the hypothesis that each functional gene set is more or less highly ranked (one-sided Wilcoxon rank-sum).

Results: To our knowledge, this is the first array profiling study using LCM FFPE material in UroCa patients. Of 38 samples, 30 (15 Prog, 15 Nprog) showed excellent hybridization characteristics as demonstrated by wide dynamic signal range across probes. Sample age had no effect on assay parameters ($p>0.87$). 145 genes were differentially expressed (adj. $p<0.05$) between Prog and NProg. Overall, Notch pathway components were most significantly associated with progression ($p<.04$). Among treated patients, components of the androgen receptor signaling pathway were most significantly associated with progression (adj. $p<0.006$), including sorbitol dehydrogenase (SORD), a well established direct target of AR. This observation held despite Prog and NProg being being overwhelmingly male (88%, 84%, respectively, n.s.).

Conclusions: Comprehensive gene expression profiling on LCM samples is feasible, even after long periods of follow-up. OUr data implicate signaling by the Notch and AR pathways in bladder cancer progression and suggest molecular targets for risk stratification and therapeutic intervention. Confirmatory studies in larger cohorts are ongoing.

1660 The Effects of Neoadjuvant Chemoradiation Therapy on Microsatellite Instability and Mismatch Repair Reporting in Rectal Adenocarcinoma.

EN Bit-Ivan, JA Nowak. NorthShore University HealthSystem, Evanston, IL; University of Chicago Pritzker School of Medicine, IL.

Background: Mismatch repair protein expression and microsatellite instability (MSI) testing have become important tools in assessing patients with sporadic and inherited colorectal cancer (CRC). The predominant genes which affect DNA mismatch repair (MMR) include MLH1, MSH2, MSH6, and PMS2. MMR proteins form complexes that play an important role in maintaining fidelity during DNA replication and in recombinational repair. Their expression can be evaluated by the use of immunohistochemistry (IHC), while their function can be assessed by monitoring the stability of selected microsatellite loci.

Fifteen to 20% of all colorectal adenocarcinomas display defective MMR. The majority of deficient MMR is due to gene silencing by promoter hypermethylation (sporadic CRC). Approximately 2 to 5% of CRC are due to inherited mutations in the MMR genes, a manifestation of Lynch Syndrome, an autosomal dominant disorder which has clinical and prognostic implications.

The evaluation of tumors for MSI status and MMR expression is typically performed on excised specimens. Some patients, however, are treated with chemoradiation prior to surgery. Choi et al (Int J Radiat Oncol Biol Phys 68(5):1584 (2007)) recently reported that presurgical chemoradiation therapy can suppress or induce mismatch repair, potentially influencing the reliability of MSI and MMR evaluation performed on those specimens. The purpose of this study is to determine the effect of chemoradiation on MMR protein expression and MSI testing in CRC.

Design: Twenty patients with CRC who received presurgical chemoradiation between 7/05 and 7/10 were identified in our surgical pathology archives. Paraffin embedded pre-treatment and post-treatment samples were reviewed and evaluated to determine MSI status and MMR protein expression.

Results: Eighteen of 20 pre-treatment tumor specimens were classified as microsatellite stable (MSS) using a panel of five recommended mononucleotide microsatellite markers. One tumor exhibited instability in only one marker (MSI-L) and another tumor exhibited instability in two markers (MSI-H). All pre-treatment specimens demonstrated expression of the four MMR associated proteins by IHC analysis. Evaluation of postsurgical specimens showed no change in MSI status or expression of MMR proteins.

Conclusions: Our data do not support the hypothesis that neoadjuvant chemoradiation can change MMR status of tumors as determined by MSI testing or MMR protein expression.

1661 Do Inflammatory Myofibroblastic Tumors (IMT) and IgG4 Related Lymphoplasmacytic Sclerosing Lesions (IgG4-RLSL) Have a Similar Pathogenesis?

SJ Bokhari, JF Silverman, A Mohanty. Allegheny General Hospital, Pittsburgh, PA.

Background: IgG4-RLSLs is most frequently described in the pancreas and salivary gland, but have also been recently reported with increasing frequency in a variety of body sites. Diagnostic histologic features of IgG4-RLSL include infiltration of plasma cells that express IgG4, areas of dense sclerosis and phlebitis. Some of these morphologic features are also shared by IMTs, including the presence of numerous plasma cells and fibrosis. While IgG4 plays a central role in IgG4-RLSLs, there is scant literature evaluating the role of IgG4 in IMT. We studied the presence of IgG4 positive plasma cells in IMT to determine if it possibly shares a possible common pathogenesis with IgG4-RLSL.

Design: A total of 16 cases of IMTs with H&E slides and corresponding tissue blocks were retrieved from the hospital computer system. All selected cases had been previously confirmed as IMTs by histology and immunohistochemistry (IHC) panel that included smooth-muscle actin and anaplastic-lymphoma kinase (ALK). In addition, IHC for IgG4 was also performed on tissue-block sections that were formalin-fixed and paraffin embedded, using a heat-induced epitope retrieval technique.

Results: 16 IMTs were included in our study from the following sites: 5/16 from the orbit, 3/16 from the lung, 2/16 from the kidney, and one each from the liver, breast, colon, bladder, small intestine, and lymph node. 15/16 (93.8%) IMTs demonstrated IgG4 positive plasma cells. Of these 15 cases, 11/15 (73.3%) showed at least 90% of all plasma cells being positive for IgG4, 2/15 (13.3%) showed at least 50% of all plasma cells being positive for IgG4, and 2/15 (13.3%) showed at least 20% of all plasma cells being positive for IgG4. All cases showing at least 90% of plasma cell positivity for IgG4 demonstrated both strong membranous and cytoplasmic staining. 7/15 (46.7%) were ALK negative, and 8/15 (53.3%) were ALK positive. Pattern and intensity of staining was identical in the ALK negative and ALK positive cases. A single IMT in our study was negative for IgG4 and ALK.

Conclusions: Our results indicate that IMTs contain a significant number of IgG4 positive plasma cells. These findings raise the possibility that IMTs and IgG4-RLSLs not only can show similar morphologic features characterized by inflammation and sclerosis, but may also share a common pathogenesis.

1662 *SOX2* Amplification Is a Common Event in Squamous Cell Carcinomas of Different Organ Sites.

M Braun, S Maier, T Wilbertz, V Scheble, M Reischl, R Mikut, R Menon, P Nikolov, K Petersen, C Beschorner, H Moch, C Kakies, C Protzel, J Bauer, A Soltermann, F Fend, A Staebler, C Lengerke, S Perner. University Hospital Bonn, Germany; University Hospital Tuebingen, Germany; Research Center Karlsruhe, Karlsruhe, Germany; University Hospital Zurich, Switzerland; University Hospital Rostock, Germany.

Background: Acquired chromosomal aberrations, including gene copy number alterations, are involved in the development and progression of human malignancies. *SOX2*, a transcription factor-coding gene located at 3q26.33, is known to be recurrently and specifically amplified in squamous cell carcinomas (SCCs) of the lung, the esophagus and the oral cavity. In these organs, the SOX2 protein plays an important role in tumorigenesis and tumor survival. The aim of this study was to determine whether *SOX2* amplification is also found in SCCs in other organs commonly affected by this tumor entity.

Design: Applying fluorescence in-situ hybridization, we assessed SCCs of the cervix uteri (n=47), the skin (n=57) and the penis (n=53) for *SOX2* copy number alterations.

Furthermore, we performed immunohistochemical SOX2 staining to assess SOX2 protein expression. For quantification of protein expression, semi-automated quantitative image analysis software was applied to obtain a continuous spectrum of average brown staining intensity.
Results: We detected *SOX2* amplifications in 28% of cervical SCCs, 28% of skin SCCs, and 32% of penile SCCs. Moreover, we found that the *SOX2* amplification is significantly associated with an overexpression of the corresponding protein in SCCs ($p<0.001$).
Conclusions: In our current study we could show that amplification of *SOX2* and consequent overexpression of the corresponding protein are not confined to lung SCCs, but that they are found in a considerable subset of SCCs in different organ sites, i.e. the uterine cervix, the skin and the penis. Our data emphasize the need for further elucidation of the role of SOX2 during SCC carcinogenesis and its clinical implications.

1663 Progesterone Induces ERK 1/2 Activation and AP-1 DNA Binding Activity through a Mechanisms Involving Src Kinase and EGFR Transactivation in MCF-7 Breast Cancer Cell.

F Candanedo Gonzalez, P Cotes Reynosa, A Soto Guzman, M Guaderrama, T Robledo, E Perez Salazar. CINVESTAV-IPN, Mexico City, DF, Mexico.
Background: In Mexico, breast cancer is the second most frequent malignancy and occurs in 46% of cases of women younger than 50 years of age. About 75% of breast tumors are positive for the progesterone receptor (PgR) which is expressed in several breast cancer cell lines and its stimulation with progesterone induces cell proliferation. However, the signal transduction pathways activated by progesterone have not been studied in detail. The activating protein-1 (AP-1) transcription factor transduces growth signals through signal transduction pathways to the nucleus, leading to the expression of genes involved in growth and malignant transformation in many cell types. In order to elucidate the signaling pathways whereby progesterone modulate cell proliferation, we investigated the effects of progesterone administration on AP-1 expression. We hypothesized that PgR induced activation of AP-1 transcription factor to induced the growth of breast cancer cells.
Design: To determine whether PgR modulates the AP-1 DNA binding, MCF7 breast cancer cells were treated with progesterone (100 nM) for 30 min and evaluated by electrophoretic mobility shift assay, Wstern blot and proliferative assays.
Results: Our results demosntrate that stimulation of MCF-7 cells with progesterone hormone promote the rapidly phosphorylation of ERK 1/2 at Thr-202 and Tyr-204 and the formation of AP-1-DNA complex in a fashion dependent of Src kinase activity and EGFR transactivation. Furthermore, proliferation induced by progesterone is restricted to breast cancer cells in a fashion dependent of ER1/2 and AP-1 activation.
Conclusions: These results suggest that some the progesterone effects in breast cells are mediated through induction of AP-1 complex expression and consequently through modulation of the AP-1 dependent gene expression. Our data indicate that proliferation induced by progesterone is restricted to breast cancer cells, and that ERK1/2 activation and AP-1-DNA complex formation are mediated by Src family kinases and transactivation of EGFR.

1664 Perineural Invasion or Neurogenesis?

AM Cano-Valdez, N Cruz-Viruel, H Dominguez-Malagon. Instituto Nacional de Cancerologia, Mexico City, Mexico; Hospital Juarez de Mexico, Mexico City, Mexico.
Background: Perineural invasion (PNI) is a common phenomenon frequently observed in carcinomas of several organs and in some tumors is considered a prognostic factor for recurrence after surgical treatment. Together with PNI we have frequently observed nerve hypertrophy (NH). That 's why we postulate that nerve fibers may be produced in situ or their growth may be stimulated by neoplastic factors that induce nerve proliferation and hypertrophy. To investigate this possibility, we examined the size of nerve fibers and the expression of diverse growth factors and nerve markers in a group of carcinomas with PNI.
Design: Thirty six cases of carcinomas with PNI and nerve fiber hypertrophy (NH) were collected (Group I), and compared with 23 cases neither PNI nor NH (Group II). The paraffin blocks were selected and tissue microarrays were performed. Immunohistochemical studies were done on tissue macroarrays ("microchops") using antibodies against: low-affinity nerve growth receptor p75NTR (CD56), S-100 protein, platelet derived growth factor receptor (PDGFR) and epithelial growth factor receptor (EGFR). Comparative analysis of expression in both groups and the presence of NH were done and statistical analysis was performed using student T test.
Results: NH and PNI were easily seen on routine slides in all cases of Group I, while only 3 cases of Group II showed H&E visible nerve fibers, and they required S-100 protein to highlight them. Average nerve size was 0.23cm in group I, whereas 0.018cm nerve thick was observed in control group. A greater NGFR expression was observed in group I (47% vs 23%). However, statistical difference wasn't significant. No differences were found with S100, PDGF and EGFR.
Conclusions: Our findings don't support the neurogenesis theory. However, use of therapies directed against tumoral neurotrophins as potential molecular targets may be useful to limit recurrence, dissemination and in consequence, to improve survival. Nevertheless, it is necessary to carry out more studies analyzing other factors of nervous growth to support this theory.

1665 Acid Increases P16 Methylation Via Activation of NADPH Oxidase NOX5-S in Barrett's Esophageal Adenocarcinoma Cells.

W Cao, J Hong, J Behar, LJ Wang, J Wands, RA DeLellis, M Resnick. Rhode Island Hospital and Warren Alpert Medical School of Brown University, Providence.
Background: Gastroesophageal reflux disease(GERD) complicated by Barrett's esophagus (BE) is a major risk factor for esophageal adenocarcinoma (EA). However, the mechanisms of the progression from BE (intestinal metaplasia) to EA are not fully understood. Inactivation of the tumor suppressor gene p16 may play an important role in this progression. Hypermethylation of the p16 promoter is an important mechanism for inactivating p16. In this study we examined whether acid increases methylation of the p16 gene promoter by activating NADPH oxidase NOX5-S in an EA cell line OE33.
Design: P16 mRNA and methylation of p16 promoter were measured by real-time PCR. Transfection of NOX5 siRNA and plasmid was carried out by using Lipofectamine 2000 and Amaxa-Nucleofector-System respectively.
Results: P16 methylation was significantly increased in OE33 cells when compared with Barrett's cell line BAR-T and squamous cell line HET-1A. Acid treatment significantly increased methylation of p16 promoter and decreased the p16 mRNA level. OE33 cells expressed NADPH oxidase NOX5-S. Acid-induced increase in H_2O_2 production was significantly reduced by knockdown of NOX5-S. Knockdown of NOX5-S significantly increased p16 mRNA, inhibited acid-induced down-regulation of p16 mRNA. Knockdown of NOX5-S also blocked the acid-induced increase in p16 methylation. Conversely, overexpression of NOX5-S and exogenous H_2O_2 significantly decreased p16 mRNA and increased p16 methylation.
Conclusions: NOX5-S is involved in acid-induced hypermethylation of the p16 gene promoter and in downregulation of p16 mRNA. It is possible that acid reflux in BE patients may activate NOX5-S. NOX5-S-derived ROS in turn increases p16 promoter methylation and down-regulates p16 expression, thereby contributing to the progression from BE to EA. Supported by NIH NIDDK R01 DK080703.

1666 PI3K/mTOR Signaling Regulates Prostatic Tubulogenesis.

S Ghosh, H Lau, B Simons, D Berman, TL Lotan. Johns Hopkins University School of Medicine, Baltimore, MD.
Background: The Gleason grading system, one of the most powerful prognosticators in prostatic adenocarcinoma, is a measure of the degree to which tumor cells form tubules. However the signaling pathways that modulate normal and malignant prostatic tubulogenesis remain unclear. Here, we used embryonic prostatic development as a model system to study the role of the oncogenic PI3K/mTOR signaling pathway in the regulation of prostatic tubulogenesis and cell migration.
Design: Urogenital sinuses (UGS) were dissected from E15.5 mice and prostatic branching morphogenesis was initiated in the presence of PI3K/mTOR inhibitors or vehicle. Immunoblotting, immunohistochemistry (IHC) and immunofluorescence (IF) in mice transgenic for AKT-PH-GFP were used to measure PI3K/mTOR activity during prostatic development *in vivo* and following drug addition *in vitro*. A novel mesenchyme-free epithelial culture system was used to quantify prostatic epithelial migration during branching. (ER)-ROSA-cre $PTEN^{loxp/loxp}$ mice were used to study the effects of PTEN loss of function during tubulogenesis.
Results: Immunoblotting, IHC and IF demonstrated that PI3K is induced and activated in the invading epithelium during prostatic tubulogenesis. UGS organ culture in the presence of LY294002 or wortmannin (PI3K inhibitors) resulted in a significant decrease in epithelial bud number and length. Surprisingly, this decrease in prostatic branching was not due to changes in cellular proliferation or apoptosis. Instead, PI3K inhibition resulted in defective prostate epithelial cell migration, with markedly decreased cellular displacement and speed. Interestingly, simultaneous inhibition of mTORC1 and C2 phenocopied PI3K inhibition, suggesting that mTOR is the essential downstream mediator of PI3K signaling in prostatic tubulogenesis. Remarkably, however, mTORC1 inhibition alone had the opposite effect, increasing bud number and length. Although PTEN loss of function in UGS cultures resulted in increased PI3K signaling, there was no change in prostate branching likely because downstream mTORC1 and C2 activity have opposite and competing effects.
Conclusions: Loss of PTEN frequently results in aberrant PI3K/mTOR signaling during prostatic tumorigenesis. Using embryonic development as a model system, we found that this signaling pathway is required for prostatic epithelial tubulogenesis and cell migration. Significantly, the major downstream effectors of PI3K signaling, mTORC1 and C2, have opposing effects on prostatic tubulogenesis, suggesting that drugs that preferentially inhibit mTORC2 activity may be useful in the treatment of prostate carcinoma.

1667 Furin Expression in Seminal Vesicle. Any Impact on Prostate Cancer Development?

Y Gong, C Torres, C Sell, A Bitto, J Fu, AJ Klein-Szanto, FU Garcia. Drexel University College of Medicine, Philadelphia, PA; Fox Chase Cancer Center, Philadelphia, PA.
Background: Prostate and seminal vesicle (SV) are organs that are anatomically and functionally related. However, while prostate cancer (PCa) is very common in older men, the SV rarely develops cancer. The fact that two closely related organs have such different cancer rates offers an opportunity to study potential underlying molecular interactions that determine cancer development exclusively in prostate. There is little information characterizing the SV in terms of proliferation and senescence and the possible impact on PCa development. Furin, a calcium dependent serine proteinase, has been shown to be over expressed in a variety of cancer cells and selectively activate IGF-1 and IGF-1 receptor by limited protein digestion. We propose to study the expression of Furin and to characterize senescence in SV on different age groups using two well-established markers P21 and P16.
Design: Immunofluorescence for P21 and P16 and immunohistochemistry (IHC) for Furin were evaluated in SV of two different age groups (younger < 60 and older ≥60 years) (n=9 in each group). Tissue microarrays from 23 de-identified radical prostatectomy specimens with duplicate cores from benign glands, PCa and SV were constructed. Furin, PTEN, P53 and Ki-67 expression levels were evaluated by IHC using image analysis. Both P21 and P16 were quantified manually. Expression was compared using t-test.

Results: P16 and P21 expression levels are increased significantly during SV aging. P16 is expressed in 19.2% of epithelial cells in the younger group and 42.4% in the older group ($p<0.05$). P21 is expressed in 13.3% of epithelial cells and 49.1% in the older group ($p<0.05$). Furin is highly expressed in the luminal cells of SV and SV fluid and there is increased expression during aging, Immunoscore (IS): 193.8 in younger group and 233.9 in the older group, $p<0.05$). However, within the prostate, Furin expression is highest in atrophic glands, followed by high-grade prostatic intraepithelial neoplasm (HGPIN) and PCa. PTEN expression is low in PCa cells, IS: 42.8 when compare to benign glands, IS: 62.3 ($p<0.05$) and SV, IS: 75.4 ($p<0.05$). Ki-67 has an opposite expression pattern. P53 expression is low in all areas.
Conclusions: 1) SV senescent cell population increases with age. 2) Furin expression is increased during aging in SV. 3) Furin is present in prostatic atrophy and HGPIN. 4) We propose that increases in the population of senescent cells within SV during aging, changes their secretory pattern by increasing Furin expression.

1668 Neurotensin Receptor 1 (NTSR1) Expression in Inflammatory Bowel Diseases (IBD): Association with Mucosal Inflammation and Dysplasia/Neoplasia.

X Gui, S Liu, Z-H Gao. University of Calgary, AB, Canada.
Background: Neurotensin (NT), a 13-AA gut peptide, acts as paracrine and endocrine modulator of various gut functions. Most of NT's effects are mediated through high-affinity neurotensin receptor 1 (NTSR1), a member of G-protein-coupled receptor family. NT/NTSR1 signaling was found to be proinflammatory as well as proregenerative in colonic inflammation. NTSR1 is also involved in the tumorigenesis and progression of colonic carcinoma, mainly via its link with *Wnt/APC/Tcf*/β-*catenin* pathway. It is our hypothesis that NTSR1 in colonic epithelium is upregulated in IBD and NTSR1 overexpression plays a role in the development of colitis-associated dysplasia/neoplasia.
Design: 18 colectomy cases of long-standing IBD (13 UC, 3 CD, 2 IC, 14 M, 4 F, age 26-84 yo) were retrieved from our pathology file. Of each case, tissue blocks were selected from those with proven histology of normal (3), active colitis (16), inactive colitis (14), raised low-grade dysplasia (LGD, 16), high-grade dysplasia (HGD, 3), and adenocarcinoma (CA, 8). Of LGD lesions, a distinction between dysplasia-associated lesion or mass (DALM, i.e., sessile full-thickness dysplasia, colitis-associated, 12) and adenoma-like dysplastic polyps (ALDP, i.e., 'top-down' pattern dysplasia, likely sporadic adenoma, 4) was attempted based on current morphological criterion. NTSR1 expression was detected by immunohistochemistry, and it was semiquantitated (as negative, 1+, 2+, and 3+).
Results: Immunoreactivity of NTSR1 appeared in a cytoplasmic pattern. NTSR1 was not detected in normal mucosa but was expressed similarly in both active and inactive colitis. LGD showed a significantly stronger expression as compared with non-dysplastic colitic mucosa, with most cases showing a ≥ 2+ intensity (81.25% *vs* 32.26%, p = 0.001) but less cases showing a 1+ intensity (18.75% *vs* 64.52%, p = 0.07). However, no significant difference existed between DALM and ALDP. CA or combined CA/HGD showed a further stronger expression, with more cases showing a 3+ intensity than that in LGD of both DALM and ALDP (62.50% *vs* 12.50% for CA *vs* LGD, p = 0.037; 63.64% *vs* 12.50% for CA/HGD *vs* LGD, p = 0.021).
Conclusions: Both active and inactive colitis upregulate NTSR1 of colonic epithelium. Low to high-grade dysplasia and carcinoma are associated with a step-wisely higher expression. The overexpression shows a similar pattern in both colitis-associated and sporadic dysplasia, which suggests that NTSR1 may be equally involved in these two dysplastic/neoplastic processes.

1669 Neurotensin Receptor 1 (NTSR1) Is Preferentially Expressed in Glandular Element of Intestinal Tumors with Neuroendocrine Differentiation.

X Gui, Y Li, S Liu, Z-H Gao. University of Calgary, AB, Canada.
Background: Neurotensin (NT) is a gut neuroendocrine peptide with diverse functions including trophic effects. Most of NT's effects are mediated via the high-affinity neurotensin receptor 1 (NTSR1), a member of G-protein-coupled receptor family. Both NT and NTSR1 express in several carcinomas as well as neuroendocrine tumors. In GI tract, certain tumors, *e.g.*, goblet cell carcinoids (GCCs) and glandular-endocrine mixed tumors (GEMTs), show dual differentiation with a presentation of mixed glandular and endocrine features. The expression pattern and oncogenic role of NTSR1 in this type of GI tumors are not yet understood. Here we studied whether NTSR1 expression shows a preference in one of the differentiations.
Design: NTSR1 expression was detected by immunohistochemistry in appendicieal GCCs (n=17, 8 M, 9 F, age 22-69 yo), appendiceal/ileal classic carcinoid tumors (CCTs) (n=10, 5 M, 5 F, age 13-86 yo), and colorectal GEMTs including composite tumors (n=12, 5 M, 7 F, age 39-85 yo) and collision tumors (n = 10, 5 M, 5 F, age 48-74 yo). Conventional colorectal adenocarcinomas (CRCs) without neuroendocrine features (n=12, 7 M, 5 F, age 42-85 yo) were included as an additional control. The intensity/degree of NTSR1 expression was semiquantitated (as negative, 1+, 2+, 3+). A comparison of NTSR1 expressions was analyzed between different tumors and between glandular and endocrine elements of GEMTs.
Results: Immunoreactivity of NTSR1 appeared in a cytoplasmic granular pattern. As compared with CCTs, GCCs showed a significantly higher positivity (94.1% *vs* 70%, p < 0.05) and higher intensity (2+, 35.3% *vs* 0%, p < 0.05) of NTSR1 expression. 5 GCCs with marked adenocarcinoma-like pattern all showed a 2+ to 3+ expression. In GEMTs, the collective positivity of NTSR1 is significantly higher in glandular elements than that in endocrine elements (70.6% *vs* 38.1%, p < 0.05), and the difference seems to exist mainly in collision tumors as compared with composite tumors. In composite tumors both glandular and endocrine tumor cells showed a similar positivity. In comparison, all CRCs showed an outstandingly higher level expression (90% with 3+, 10% with 2+).
Conclusions: In various intestinal tumors, NTSR1 expression is significantly stronger in the tumor cells with glandular differentiation than in that with neuroendocrine differentiation. Our data suggests that NTSR1 is preferentially involved in the carcinogenesis and/or progression of adenocarcinomas. This finding may have therapeutic implication.

1670 Carcinogen-Induced Breast Cancer Prevention by Ingestion of Stearate.

RW Hardy, E Toline, LM Evans, R Desmond, A Ibrahim-Hashim, GP Siegal. University of Alabama at Birmingham.
Background: Dietary stearate has been previously shown to reduce breast cancer tumor & metastatic burden in an orthotopic mouse model. The goal of the study was to test the effectiveness of dietary stearate at inhibiting breast cancer development in a carcinogen induced breast cancer model. We selected the N-nitroso-N-methylurea (NMU) rat carcinogen induced model because it is direct acting, does not require host activation, and tumors generated exhibit histologic and endocrinologic features which resemble human breast cancer.
Design: Three diets were used; a 17% stearate diet, the key being that highly purified stearate was added directly to the diet, a linoleate diet containing 17% safflower oil as the source of linoleate (SF) and a low fat control diet (LF) with a reduced amount of fat (5%) from corn oil. Corn oil contains a mix of linoleate and oleic acids as the major components which are, coincidently the two major non-esterified fatty acids in human serum. All 3 diets had adequate essential fatty acids and were fed to female rats treated with NMU and followed out 100 days. The diets were initiated 1 week prior to receiving NMU.
Results: There was no difference in the weight of the rats among groups throughout the study. Approximately 40% fewer animals on the stearate diet developed palpable tumors compared to the control (n=30-35 animals/diet; $p<0.05$). No difference was observed among the 3 diets as to the time for first tumor appearance. Stearate decreased the average number of tumors per rat compared to the LF (n=30-35 animals per diet; $p<0.05$) and had less tumors per rat than the SF although this was not statistically significant. Dietary stearate significantly reduced tumor burden as defined as a decreased in tumor weight by ~50% as compared to LF and SF ($p<0.001$) and large tumors as compared to the LF (~47% reduction in tumors over 0.25 g, p= 0.02). Stearate had similar results compared to the linoleate diet in terms of reduced numbers of large tumors; however they were not statistically significant. In those rats that did develop tumors, the stearate diet group had a similar number of adenocarcinomas compared to other diets; however the stearate and SF groups had lower numbers of DCIS/microinvasive disease as compared to the LF. The dietary groups had similar numbers of the other precursor lesions classified.
Conclusions: The stearate and SF diets were both effective at reducing both tumor burden and incidence in this model although stearate was the best at reducing tumor burden. Dietary stearate may be useful as an alternative/complementary therapy or preventative agent against breast cancer.

1671 Esophageal Dysmotility: A Manifestation of IgG4-Related Sclerosing Disease.

KB Johnson. Duke University Medical Center, Durham, NC.
Background: Esophageal motility disorders have a wide range of primary and secondary causes; yet, many cases remain idiopathic in etiology. When medical treatment modalities fail to control symptoms, surgical myotomy or partial esophagogastrectomy can be the only alternative. Following a sentinel case of end-stage dysmotility with markedly increased IgG4-positive plasma cells, this study was undertaken to identify at what frequency additional cases might exist.
Design: A retrospective review was performed of all esophagogastrectomies undertaken for a primary diagnosis of either dysmotility or achalasia between 2000-2010. Including the sentinel case, 10 cases were identified (excluding 4 cases of pseudoachalasia due to malignancy or fistulas). IgG4-positive and IgG-positive plasma cells were each counted in 3 high power fields (hpf) in the most concentrated areas, the average calculated and an IgG4:IgG ratio determined. A cutoff IgG4:IgG ratio of 0.3 was used to define significant elevation in the IgG4-positive plasma cells. These results were correlated with the histologic and clinical findings.
Results: Four of the 10 cases had an IgG4:IgG ratio >0.3 and differed significantly histologically from the remaining 6 cases. The IgG4-positive patients had an average age of 64 and were 25% male (vs. 54 and 50%; differences not significant). The average IgG4:IgG ratios were 0.48 (0.35-0.72) vs. 0.15 (0-0.23; p=0.005). The total average IgG4 counts were also significantly different: 207/hpf (151-287/hpf) vs. 18/hpf (0-48/hpf; p=0.004). These 4 IgG4-positive cases showed inflammation predominantly in the submucosa, with increased follicular hyperplasia (100% vs. 17%; p=0.002) and periductal inflammation (100% vs. 33%; p=0.01), but did not differ significantly with respect to the observed fibrosis, lymphocytic ductulitis, or phlebitis. One patient demonstrated phlebitis, elevated IgG level (1710, normal 588-1573) and ANA titer (1:640). None of the patients had known IgG4-related lesions elsewhere.
Conclusions: Significantly elevated IgG4 counts, IgG4:IgG ratios, periductal inflammation and lymphoid hyperplasia were identified in 40% of our esophageal dysmotility cases over 10 years. These results suggest that some cases of esophageal dysmotility may be part of the IgG4-related sclerosing disease spectrum. If so, such patients would be expected to respond favorably to immunosuppression, obviating the need for invasive management.

1672 Evaluation of PTEN and TMPRSS2-ERG Abnormalities in Prostate Cancer by FISH and Immunohistochemistry To Address Intra- and Inter-Tissue Heterogeneity and Disease Progression.

AM Joshua, A Evans, J Squire, M Yoshimoto, O Ludkovski, S-H Tan, A Dobi, B Furusato, G Petrovics, S Srivastava, IA Sesterhenn. University of Toronto, ON, Canada; Toronto General Hospital, ON, Canada; Queens University, Kingston, ON, Canada; USUHS, Rockville, MD; Armed Forces Institute of Pathology, Washington, DC.

Background: Gene fusions involving the ERG oncogene and deletions of the PTEN tumor suppressor gene are frequent alterations in prostate cancer. Recent reports highlighted the cooperation of these two pathways in prostate cancer progression using mouse models. Our laboratory developed a specific monoclonal antibody (ERG MAb) recognizing the ERG oncoprotein in human prostate tissue. The objective of this study was to determine the frequency of ERG positive prostate cancer by immunohistochemistry (IHC) compared to ERG gene fusion frequency by fluorescent in situ hybridization (FISH), their association with PTEN deletion, and correlation with clinico-pathological parameters of disease progression.

Design: A tissue microarray (TMA) was constructed from 142 radical prostatectomy (RP) specimens with usual acinar-type prostate carcinoma obtained at University Health Network (UHN) between 2001 and 2002 comprising 724 spots. The TMA was constructed using up to six 0.6 mm donor cores from each RP specimen. In cases of multi focal and bilateral carcinoma, 3 donor cores were obtained from the largest foci in each lobe. Distinct tumor foci were defined as those separated by a distance of > 3mm on a single slide or > 4 mm in adjacent blocks. Different Gleason patterns were also sampled within each focus. Standard clinical follow-up data, representing 7-9 years of follow-up, were compiled for each case using a UHN RP clinical database.

Results: Heterogeneity within the PTEN locus was widespread. An association between ERG protein expression and PTEN deletions was apparent. Among prostate tumors with wild type PTEN 45% was ERG positive, while 57% of the PTEN hemizygous, and 77% of the PTEN homozygous cases were ERG positive, respectively. Correlation with clinical outcomes, such as biochemical progression, is ongoing and will be presented.

Conclusions: We conclude that ERG IHC is an emerging diagnostic modality that may help the assessment of ERG status in prostate tumors. PTEN interaction with ERG status may reveal clinical insights and allow prognostic genomic grading in prostatic carcinogenesis. Further validation studies are needed.

1673 Hypoxia-Related Protein Expression and Its Clinicopathologic Implication in Carcinoma of Unknown Primary.

JS Koo, H Kim. Yonsei University Health System, Seoul, Korea; Seoul National University Bundang Hospital, Seongnam, Korea.

Background: Carcinoma of unknown primary (CUP) is a heterogeneous entity with different clinical and histological features. The aim of this study was to investigate the clinicopathological features and expression of proteins associated with carcinogenesis and tumour environment in different histological subtypes of CUP.

Design: Sixty-nine cases of CUP were subjected to immunohistochemistry for EGFR, HER-2, p53, ERCC1, RRM1, REDD1, HIF1α, COX-2, GLUT-1, 14-3-3σ, Phospho-mTOR, Phospho-S6, AMPKα1, Phospho-Akt, PDGF-β receptor, and caveolin-1, and fluorescence in situ hybridisation for HER-2 gene amplification.

Results: Fourteen (20.3%) cases were poorly differentiated carcinoma (PD), 24 (34.8%) were adenocarcinoma (AD), 17 (24.6%) were squamous cell carcinoma (SC) and 14 (20.3%) were undifferentiated carcinoma (UD). AD were mostly carcinomatosis type, while SC and UD were mostly nodal type (p<0.001). SC showed more frequent EGFR overexpression (p<0.001) and Glut-1 (p=0.001). AD (p=0.001) and carcinomatosis (p<0.001) types showed shorter overall survival. SCs expressing Glut-1, HIF1α and COX2 showed a poor prognosis (p=0.048, 0.029, and 0.042, respectively).

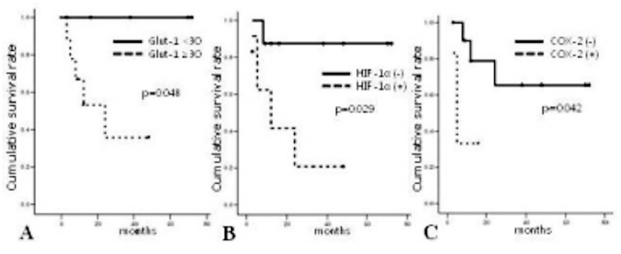

Conclusions: CUP shows various clinicopathological features according to the histological subtypes. SC is mainly associated with nodal metastasis in the head and neck, and frequent EGFR overexpression and Glut-1 expression. Glut-1, HIF1α and COX2 expression in SC is associated with a poor prognosis.

1674 Autophagic Vacuolization as a Mechanism for Proteinuria-Induced Proximal Tubulopathy in the PEXTKO Mouse.

DR LaFrance, G Rhodes, B Molitoris, DJ McCarthy, KJ McCarthy. LSU Health Sciences Center, Shreveport, LA; Indiana University Purdue University at Indianpolis.

Background: Albuminuria in glomerular diseases has been attributed to the loss of glomerular basement membrane (GBM) heparan sulfate (HS), which is recapitulated in the PEXTKO mouse model (Kidney Int. 74:289-99), whose GBM lack significant amounts of HS. Although they have a normal lifespan, PEXTKO mice develop vacuolated proximal tubule epithelium (PTE) and microalbuminuria. Similar PTE vacuoles have been described in diabetes, light chain disease and other stress-inducing nephropathies; however, the mechanism for vacuole formation remains elusive. The purpose of this study was to investigate the pathophysiology of proteinuria-induced proximal tubulopathy.

Design: Paraffin-embedded kidney sections (6 PEXTKO, 6 controls) were evaluated for apoptosis and autophagy using TUNEL assay (Promega, Madison, WI) and anti-LC3 (Novus biologicals, Littleton, CO), respectively. Additionally, multiphoton microscopy studies were conducted by labeling kidneys of anesthetized PEXTKO mice with Hoechst 33342 nuclear stain, followed by a bolus of Texas Red-labeled albumin. Kidneys were imaged with a 60x water objective lens; albumin delivery and uptake into the proximal tubules was monitored using time lapse-z step image collection.

Results: Cytoplasmic vacuoles within PTE of HS-deficient mice were identified on light microscopy.

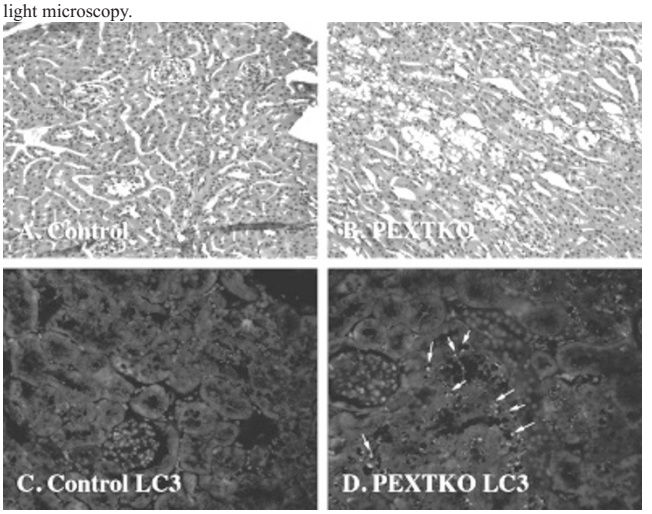

Multiphoton microscopy studies documented the inability of vacuolated proximal tubule cells to absorb albumin as compared to non-vacuolated PTE in the same animals. TUNEL results indicated no significant increase in apoptosis of PEXTKO tubules (15.17 vs. 11.02 apoptotic cells/mm^2 tubular area; p=0.11). Vacuolated PTE were positive for cytoplasmic LC3 suggesting autophagy as a mechanism of vacuole formation.

Conclusions: Protein overload eventually results in proximal tubulopathy evidenced by vacuole formation. The development of microalbuminuria (and vacuole formation) in HS-deficient PEXTKO mice is not due to loss of proximal tubule cells through apoptosis. Rather, our data suggests that proximal tubulopathy may be due to formation of autophagic vacuoles as a result of increased cell stress in response to proteinuria.

1675 The Use of Infrared Spectral Histopathology and Cytopathology.

NV Laver, BL Bird, JM Schubert, M Miljkovic, K Bedrossian, M Diem. Tufts Medical Center, Boston, MA; Northeastern University, Boston, MA.

Background: Infrared micro-spectral imaging (IRMSI) is a novel optical technique that can provide a rapid measurement of sample biochemistry and identify variations that occur between healthy and abnormal cells and tissues. The advantage of this method is that it is objective and provides reproducible results, independent of fatigue, experience and inter-observer variability. This abstract provides a review of this technology applied to both cytology (Spectral Cytopatholgy, SCP) and histology (Spectral Histopathology, SHP) samples.

Design: Unstained tissue or exfoliated cells are prepared onto infrared (IR) microscope slides and analysed by IRMSI. Specimens were interrogated by a beam of IR light that samples pixels (6.25 μm x 6.25 μm in size) from areas of interest. Each recorded IR image may consist between 25,000 and 500,000 complete IR spectra that describe the discrete biochemistry of the sample at each pixel co-ordinate. Mutlivariate methods of data analysis are used to classify and diagnose the sample spectra correlated against conventional histopathology, cytopathology, IHC and viral DNA testing.

Results: Proof of concept studies have been done on various specimen types by use of SHP. These include tissue sections from cervix, breast, colon, oral, nasopharynx, lung, thyroid and lymph nodes. More recent studies have focused on the application of this technique on Fine Needle Aspirate (FNA) specimens. Currently, acquistion of spectral images from tissue micro-arrays with high patient numbers is underway to develop a robust automated spectral method for lung cancer typing. Similar studies have been done on cervical, bladder, nasopharyngeal, and oral exfoliated samples by use of SCP. Present investigations are focused on the identification of pre-cancerous stages of disease and the detection of viral infections in squamous cells of the oral cavity and cervix.

Conclusions: SCP can identify small but reproducible biochemical changes within normal and dysplastic squamous cells. This technique may aid in the diagnosis of dysplasia when the morphology is equivocal or identify pre-dysplastic changes in normal-appearing cells. In addition, SCP has distinct potential to identify the presense of viral DNA. Primary or metastatic tissues can be detected and imaged readily in biopsy tissue sections by SHP. The resulting diagnostic images can recognize micro-metastases, tissue desmoplasia, inflammatory cells and various cancer types. Optimised IR imaging instruments may allow the acquisition and diagnosis of clinical samples within a few minutes.

1676 Merkel Cell Polyomavirus Detection in Extrapulmonary Small Cell Carcinoma.

JA Lefferts, KC Hourdequin, WA Hitzelberger, LJ Tafe, JM Pipas, MS Ernstoff, GJ Tsongalis. Dartmouth-Hitchcock Medical Center and Dartmouth Medical School, Lebanon, NH.

Background: A recently discovered polyomavirus associated with Merkel Cell carcinoma (MCC) has been termed Merkel Cell Polyomavirus (MCPyV). MCPyV is integrated in the tumor genome of Merkel Cell cancers and can be detected in 80% of MCC cases. Subsequent studies found that the virus could be detected in a smaller percentage of squamous cell and basal cell carcinomas but the virus was infrequently detected in other small cell or neuroendocrine lung carcinoma, which shares histological features with MCC. We investigated the presence of MCPyV in cases of extrapulmonary small cell carcinoma (ESCC), which also shares histological features with MCC.

Design: A search of hospital medical records yielded twenty-five cases of ESCC diagnosed between 2004 and 2009. Archived tissue was available sixteen of these cases were available for testing. Additionally eleven tissue specimens from four cases of Merkel cell carcinoma were used as positive controls. DNA samples extracted from sections of archived tissues specimens were each subjected to five separate real-time SYBR Green PCR assays for the detection of a human beta-globin gene and four MCPyV genomic targets to help ensure MCPyV detection despite possible variations in the viral genome.

Results: MCPyV DNA was detected in 3/16 (18.75%) of the ESCC samples and in all 11 MCC samples (four patients). In the three MCPyV-positive ESCC cases viral target was only detected by either one or two of the PCR assays while 8/11 MCPyV-positive MCC DNA samples tested positive by either three or all four assays and the remaining three MCC samples were positive by either one or two assays. The beta-globin endogenous control was detected in all samples tested.

Conclusions: Although MCC and ESCC share many histological features, MCPyV is detected with much more frequency in MCC. The possibility of a role for MCPyV in the etiology of ESCC remains uncertain. Since only one or two of the four assays detected MCPyV DNA in a limited number of ESCC cases, additional testing including DNA sequencing will be required to help confirm these results. The failure of the other assays to detect MCPyV could be due to sequence variability in the MCPyV genome. Alternatively, inadequate analytical specificity by some of the PCR assays could have resulted in false-positive results due to the presence of viral DNA with sequence similarities to MCPyV.

1677 RAS Mutational Analysis in 9334 Solid and Hematopoietic Malignancies.

D Ma, R Luthra, SS Chen, CC Yin, RL Sargent, KP Patel, J Medeiros, Z Zuo. The U of Texas M. D. Anderson Cancer Center, Houston.

Background: Transforming mutations of *RAS* oncogenes are present in 15% of human cancers and serve as predictors for therapeutic response and tumor progression. The distribution of *RAS* mutations varies in different malignancies, suggesting that the *RAS* oncogenes function differently in various tumors. To characterize the variable frequency and site distribution of *RAS* mutations, we identified and reviewed 9334 solid and hematopoietic malignancies tested for *KRAS* and *NRAS* mutations within our institution from 2000-2010.

Design: Genomic DNA was isolated from bone marrow, peripheral blood or micro-dissected formalin-fixed, paraffin-embedded tissue patient samples. Mutational analysis of codons 12, 13, and 61 of the *KRAS* and *NRAS* genes was carried out by PCR amplification followed by pyrosequencing using the PSQ96 HS system (Biotage AB, Uppsala, Sweden).

Results: 5200 hematopoietic malignancies and 4134 solid tumors analyzed for *KRAS* and *NRAS* mutations were identified. 1037 (25%) *KRAS* and 149 (4%) *NRAS* mutations were identified in solid tumors. Of all the *RAS* mutations identified in solid tumors, 820/1186 (70%) occurred in codon 12 of *KRAS* (K12). K12 and *KRAS* codon 61 (K61) mutations were found in 156 (13%) and 61 (5%) of patients, respectively. *KRAS* mutations most frequently occurred in colon cancer (39%), followed by lung cancer (19%) and melanoma (8%). In hematopoietic malignancies, 107 (2%) *KRAS* and 300 (6%) *NRAS* mutations were documented. *NRAS* codon 12 (N12) mutations were detected in 210 cases (52%). *NRAS* codon 13 (N13) and *NRAS* 61 (N61) mutations were found in 63 (15%) and 27 (7%) cases, respectively, with the highest mutation rate seen in chronic myelomonocytic leukemia (30%), followed by acute myeloid leukemia (8%).

Conclusions: Mutations in the *RAS* oncogene family constitute a common oncogenic mechanism in cancers across different organ systems. Our study shows that the mutation frequency and site differs greatly between and within various malignancies.

1678 The sAC Antibody Profile as a Diagnostic Adjunct in the Assessment of Pigmented Lesions.

CM Magro, G Desman, J Zippin, NA Crowson, P Chadwick. Weill Cornell Medical College, New York, NY; Laboratory of Dermatopathology, New York, NY; Regional Medical Laboratory, Tulsa, OK.

Background: Melanocytic proliferations exhibit striking heterogeneity in regards to their morphology and biologic behavior. Based on prior studies which showed a distinctive pattern in hyperproliferative squamous lesions, we chose to study soluble adenylate cyclase (sAC) antibody expression in a variety of melanocytic lesions.

Design: The immunohistochemical staining procedure for SAC has been previously described. A spectrum of melanocytic lesions was assessed. Among the cases studies were benign nevi, dysplastic nevi and malignant melanoma.

Results: In benign nevi a dot-like perinuclear Golgi staining pattern in the majority of the melanocytes.

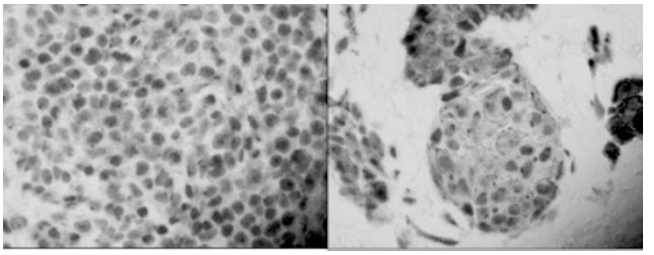

In dysplastic nevi a peri nuclear dot-like Golgi pattern analogous to the benign nevus was seen; as well with higher grade atypia a broad golgi pattern of staining was observed. In addition there was was a minor intraepidermal ccomponent with pan-nuclear staining; the number of positive staining cells showing this staining was proportionate to the degree of atypia. In malignant melanoma, extensive and prominent pan nuclear staining was noted in many cases.

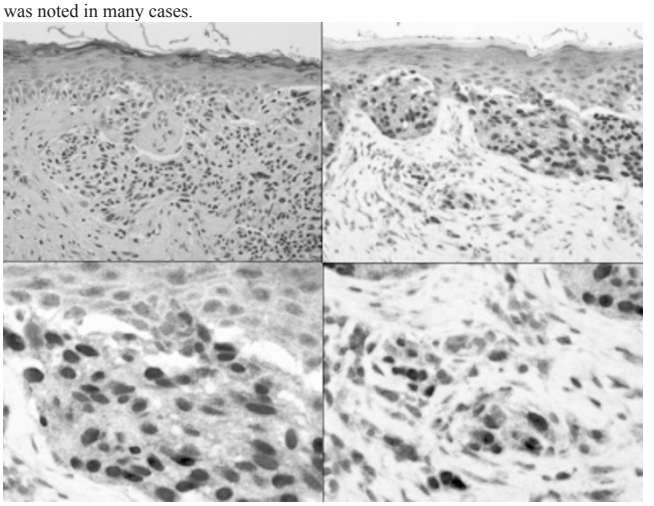

A loss of the golgi pattern was seen in several cases. The differential staining patterns aided in distinguishing capsular nevus from metastatic melanoma.

Conclusions: We found that very characteristic patterns emerged with this antibody depending on the nature of the melanocytic lesion biopsied with the hallmark of the malignant phenotype being extensive SAC expression in the nucleus with loss of golgi staining. Nuclear sAC is capable of activating CREB. Metastatic progression of melanoma is associated with overexpression and activity of nuclear CREB resulting in the down-regulation of CCN1/CYR61 expression.

1679 Degos Disease: A C5B-9 and Interferon Alpha Mediated Small Vessel Injury Syndrome.

CM Magro, JC Poe, MK Crow, L Shapiro, G Nuovo, YJ Crow, C Kim. Weill Cornell Medical College, New York, NY; Duke University Medical Center, Durham, NC; Hospital for Special Surgery, New York, NY; Albany Medical College, New York, NY; Ohio State University, Columbus; University of Manchester, United Kingdom; New York University, NY.

Background: Degos disease is small vessel angiopathy targeting the skin, gastrointestinal tract and central nervous system of unknown etiology.

Design: Skin biopsy tissues were processed for hematoxylin and eosin, immunofluorescent, MXA immunohistochemical assessment and electron microscopy studies in a patient with primary Degos disease. As well blood samples were available upon which assessment for antiendothelial cell antibodies and serum interferon alpha levels

Results: Four patients with Degos disease were encountered ranging from 2 years to 48 years. All 4 patients developed asymptomatic small cutaneous lesions complicated by severe abdominal disease. Thre of the patients died of their disease within 1 year of presentation. Skin biopsies showed a pauci-inflamatory thrombogenic microangiopathy with prominent vascular C5b-9. There was high expression of interferon-alpha, based on tissue expression of MXA, a type I interferon-inducible protein and/or an interferon gene signature in peripheral blood mononuclear cells. An obliterative fibrous mucinous arteriopathy affecting the gastrointestinal tract was noted in cases 1 through 4 and CNS in case 3. The MXA staining paralleled the extent of C5b-9 deposition.

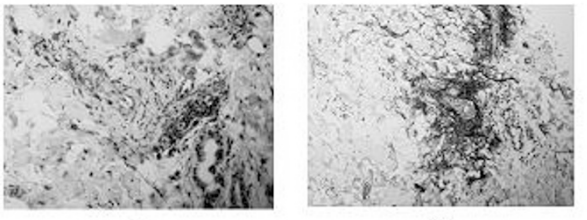

5a 5b

Conclusions: Degos disease is a distinct vascular injury syndrome affecting small vessels whereby an interferon-alpha rich microenvironment in concert with vascular C5b-9 deposition are likely causative. Complement activation is likely a direct sequelae of the local and systemic effects of interferon alpha. Improved understanding of the mechanisms of vascular injury may lead to more effective possibly with novel treatments such as with inhibitors of interferon-alpha or complement pathway activation.

1680 Susac's Syndrome: An Organ Specific Autoimmune Endotheliopathy Syndrome Associated with Antiendothelial Cell Antibodies.

CM Magro, JC Poe, M Lubow, JO Susac. Weill Cornell Medical College, New York, NY; Duke University Medical Center, Durham, NC; Ohio State University, Columbus; Neurology and Neurosurgery Associates, Winter Haven, FL.

Background: Susac's Syndrome (SS) consists of the clinical triad of encephalopathy, branch retinal artery occlusions (BRAO) and hearing loss. While it is well established that SS is due to a microangiopathy, little is known about its pathogenesis with no proven viral or environmental factors.

Design: Twelve patients with SS were encountered by JOS. Serum samples in 11 of these cases were evaluated for antiendothelial cell antibodies (AECA) by an indirect immunofluorescent assay using dermal blood microvascular endothelial cells as substrate as described below. AECA were also assessed via a Western blot technique using cutaneous endothelial cell lysates.

An archival brain biopsy was available on one of these patients. To assess for evidence of classic complement activation unstained slides were provided for C4d and C3d assessment.

Results: Based on distinctive light microscopic findings in brain biopsy material analogous to antiendothelial cell antibody mediated microvascular injury syndromes we postulated that the basis of the SS microangiopathy was one attributable to antiendothelial cell antibodies. In this regard we examined sera on 11 SS patients to assess for antiendothelial cell antibodies (AECA). Nine of the 11 patients were positive by indirect immunofluorescence and via Western blot studies using cutaneous microvascular endothelial cells as substrate.

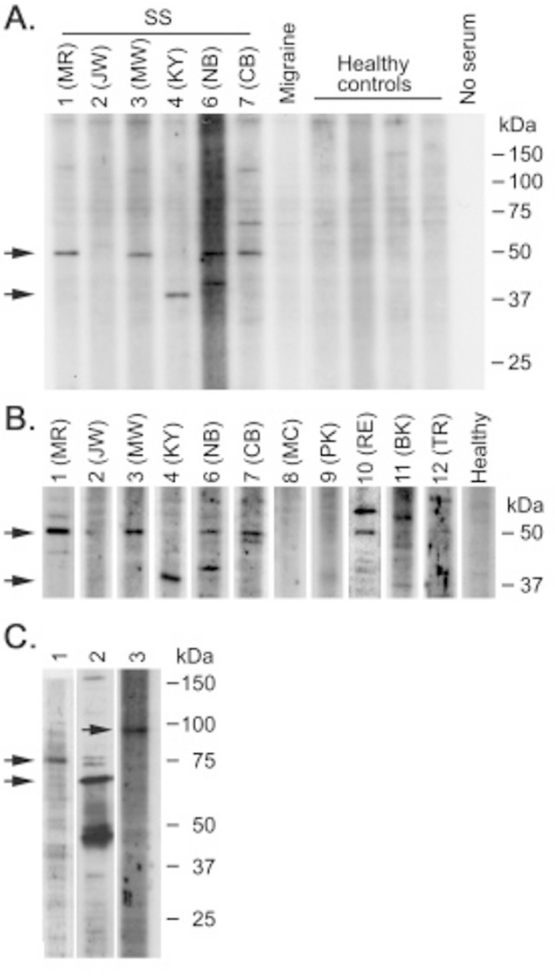

A highly distinctive band on Western blots corresponding to a 50 kilodalton (kDa) protein was observed in 8 of the 11 positive SS samples, while the serum in the other positive case exhibited specific reactivity with a protein band at 40 kDa. One of the 2 negative cases had inactive SS since 1988; the other case was an abortive variant characterized solely by BRAO.

Conclusions: Susac's syndrome is a distinct autoimmune endotheliopathy syndrome associated with antiendothelial cell antibodies: the antibody target appears to be specific in many cases and may serve as a biomarker of the disease.

1681 Suppression of Pancreatic Cancer Progression by Sulfated Non-Anticoagulant Heparin.

T Nazeer, T Sudha, T Aurumugam, M Yalcin, H Murtaza, SA Mousa. Albany Medical College, NY; Albany College of Pharmacy, Rensselaer, NY; MD Anderson Cancer Center, Houston, TX.

Background: Pancreatic cancer is the fourth most common cause of death from cancer in the United States, and its incidence is increasing. Curative treatment is still primarily surgical and is associated with significant morbidity and mortality. Recent evidences suggest that low molecular weight heparins (LMWHs) exert potent antitumor effects. The utility of heparin and LWMH as anticancer agent is limited due to effect on hemostasis. In contrast, sulfated non-anticoagulant heparins (s-NACHs) are preferable for potential clinical use because they could be administered at high dose with minimal to no effect on hemostasis. We systematically investigated the anti-tumor and anti-metastatic effect of sulfated NACH using bioluminescence imaging and histopathological studies in spontaneous metastatic mouse model of pancreatic cancer.

Design: We used luciferase-expressing MPanc96-luc to develop orthotropic pancreatic tumor mouse model. Treatment was initiated after the detection of tumor by IVIS imaging and continued for 4 weeks. s-NACH or LMWH formulation (Trinzaparin) was administered at 20 and 5 mg/kg respectively with or without Gemcitabine(GMC). Bioluminescent image guided evaluation of tumor growth and metastasis were monitored. Tumor luminescent signal intensity, tumor weight and histopahtology were assessed at the termination of the study to evaluate pancreatic cancer progression.

Results: s-NACH and LMWH efficiently inhibited tumor growth and metastasis. However, s-NACH was very effective in inducing tumor necrosis and had clear advantage over LMWH in term of bleeding side effects. GMC though reduced metastasis showed high luminescent intensity in the tumor, indicative of live tumor cells. Histological studies clearly demonstrated fewer necrotic areas in GMC treated tumors in contrast to s-NACH, which enhanced anti-tumor and anti-metastatic activities by decreasing viable cancer cells within tumor.

	Control	GMC	LMWH	NACH
Tumor wt (g)	0.71+/- 0.39	0.30+/-0.14	0.50+/-0.33	0.51+/-0.17
Luciferin signal	4.20	1.96	1.69	1.14
Necrosis (%)	17.1	3.1	30.7	49.3

Conclusions: The results demonstrate s-NACH inhibit pancreatic tumor growth in vivo without bleeding effects, reflecting its potential as an anti-tumor agent. Based on our findings, further studies to evaluate the usefulness of s-NACH as therapeutic agent in pancreatic cancer appear warranted.

1682 FoxJ1 (Ciliogenic Transcription Factor) Expression in a Variety of Tumors.

D Nonaka. The Christie NHS Foundation Trust, Manchester, United Kingdom.

Background: The motile cilia are seen in limited regions, almost exclusively in tissues where fluid movement is important for physiology, which include the upper airways and lower respiratory tract, oviduct, seminiferous tubules of the testes, and ventricles of the brain and spinal cord. Cilia are only assembled when cells exit the cell cycle from mitosis into a stationary or quiescent and differentiated state, and entry into the cell cycle is preceded by ciliary resorption. Foxj1 is pivotal for motile cilia formation and expressed in ciliated cells. Motile cilia are generally not detected at the light microscopic level in carcinoma, and its presence in certain cells generally indicates benignity.

Design: A total of 885 cases of a variety of tumors including adenocarcinomas of lung (191 cases), endometrium (56), and ovary (107) were studied for FoxJ1 immunoexpression. Extent of staining was graded as 1+, 5-25%; 2+, 25-50%; 3+, 50<%.

Results: FoxJ1 expression was frequently seen in lung adenocarcinoma (37%), ovarian adenocarcinoma of serous (84%) and endometrioid type (50%), and endometrial adenocarcinoma of serous (100%, 2/2) and endometrioid type (52%), and its expression was 1+ in the majority of the tumors. Clear cell carcinomas of both endometrium and ovary, mucinous carcinomas of the ovary were completely negative. FoxJ1 expression was seen in a few cells in gastric adenocarcinoma. FoxJ1 was negative in adenocarcinomas of breast, prostate, colon, pancreas, thyroid, and adrenal gland, hepatocellular carcinomas, urothelial carcinoma, squamous cell carcinomas of lung and head and neck, melanomas, sarcomas, seminomas, embryonal carcinomas, and yolk sac tumors.

Conclusions: Although cilia is not observed in serous papillary carcinoma at the light microscopy level, cilia differentiation can be seen in scattered tumor cells ultrastructurally. Frequent FoxJ1 expression in the majority of serous carcinomas supports the hypothesis that serous carcinoma shows differentiation toward or arises from epithelial cells of fallopian tube, which are usually ciliated. Cilia differentiation in endometrioid adenocarcinoma may represent tubal metaplasia, which is a common metaplastic change in the endometrium. Cilia can be detected ultrastructurally in 10-20% of bronchioloalveolar carcinoma. Presence of FoxJ1-positive cells in lung adenocarcinomas indicates that ciliogenesis is in progress in some tumor cells, suggesting lung adenocarcinoma can differentiate toward the epithelium of the conducting airway (bronchi).

1683 Detection of *EGFR* Mutations and Exon 19 Deletions Using Primer Extension and Fragment Analysis in a Single Reaction.

E Olsen, J Mestas, W Grody, J Deignan. University of California, Los Angeles.

Background: The epidermal growth factor receptor (EGFR) is a cellular transmembrane receptor with tyrosine kinase activity that takes part in human cancer. *EGFR* -dependent signaling is involved in cancer cell proliferation, invasion and metastasis. Targeting *EGFR* is a directed molecular approach in cancer therapy. *EGFR* inhibitors are being utilized in the chemotherapy regimens of patients with advanced non-small cell lung

cancers. Here, we have developed an assay in which we can determine the mutational status of *EGFR* in a single multiplex reaction using single-base extension and fragment analysis.
Design: Genomic DNA samples were prepared from formalin-fixed, paraffin-embedded lung tumor biopsies from the Department of Pathology at UCLA Medical Center. Analysis of the most common mutations located within exons 18, 20 and 21 of the *EGFR* gene, as well as the deletions within exon 19, was performed in a single tube by amplifying small regions flanking the mutation sites in a multiplex polymerase chain reaction (PCR). In order to determine the identity of the nucleotides at the SNP site, allele-specific fluorescently-labeled oligonucleotides were generated in a single-base extension reaction using the ABI PRISM® SNaPshot™ Multiplex Kit, and detected by capillary electrophoresis. Fragment analysis of the exon 19 deletion mutation in the same reaction was made possible by using fluorescently-labeled amplification primers for exon 19 during the multiplex PCR.
Results: The *EGFR* mutation detection assay was capable of detecting the G719S mutation in exon 18, the deletions in exon 19, the T790M mutation in exon 20, and the L858R and L861Q mutations in exon 21. The accuracy of this assay was determined by method comparison with Sanger sequencing and was found to be 100% for this limited sample. The analytical sensitivity of the *EGFR* mutation detection assay was approximately 1 ng of genomic DNA and the inter-assay and intra-assay precisions were both 100%. DNA template amounts up to 1 µg per reaction were shown not to interfere with the assay and the analytical sensitivity of the assay was determined to be ~10% mutant DNA in a wildtype background.
Conclusions: EGFR testing can be completed efficiently using a combination of primer extension and fragment analysis reactions which are relatively inexpensive to perform. This assay is capable of identifying *EGFR* mutations associated with a sensitivity or resistance to tyrosine kinase inhibitors. Such molecular information can help direct management of care in patients with advanced lung cancer.

1684 PTEN Association with mTOR Pathway Activation and Outcomes in Bladder Cancer.

M Orloff, P Elson, Y Yang, C Eng, DE Hansel. Cleveland Clinic, OH.
Background: We have recently identified increased mTOR pathway activation in urothelial carcinoma of the bladder (UCC). We next sought to determine the relationship of PTEN, an upstream negative mediator of the mTOR pathway, to mTOR activity and outcomes in UCC patients.
Design: Patients with UCC (n=118) were examined for PTEN expression, including intensity of expression (0 no expression, 1+ low, 2+ moderate, 3+ intense expression) and predominant subcellular localization (nuclear, non-nuclear). Results were correlated with the presence of lymph node (LN) metastases, recurrence-free survival (RFS) and overall survival by univariate and multivariate analysis. PTEN intron/exon mutational analysis was performed by denaturing gradient gel electrophoresis (DGGE) and mutational status was correlated with PTEN protein expression in a subset of 91 specimens.
Results: The majority of patients (91/118; 81%) demonstrated moderate to intense expression of PTEN, with PTEN loss in only 2 patients. PTEN was primarily localized to the nucleus in 30/116 (26%) patients, with some level of nuclear PTEN staining in 74/116 (64%) of patients. In LN metastases, reduced PTEN intensity was associated with an increased percentage of phospho-mTOR cells (p=0.02). PTEN mutational analysis identified 3 variants (c.132C>T, c.511C>G, c.892C>G) which were associated with absent PTEN protein expression and diffuse phospho-mTOR expression. Reduced RFS was correlated with positive surgical margins (p=0.09), carcinoma in situ (p=0.09) and nuclear PTEN (p=0.08). Reduced overall survival was significantly associated with metastases (p=0.04) and nuclear PTEN expression (p=0.04). Stepwise multivariable analysis showed an association between reduced RFS and LN metastases (p=0.03), carcinoma in situ (0.05) and nuclear PTEN (p=0.07).
Conclusions: Alterations in PTEN expression and subcellular localization appear to mediate mTOR pathway activity in bladder cancer cells, although few mutations appear to account for reduced PTEN expression. Nuclear localization of PTEN is a relatively new finding and its function in mediating cancer behavior is under investigation. Our finding of worsened outcomes with nuclear PTEN localization warrant further functional investigation.

1685 Dickkopf-1 (Dkk-1) Is a New Agonist of the Orphan Receptor Tyrosine Kinase Ror-2 in Intestinal Epithelia.

II Pacheco, J Kelly, RJ MacLeod. Kingston General Hospital and Queen's University, ON, Canada.
Background: Dickkopf-1 (Dkk-1), an evolutionary conserved glycoprotein, is a key modulator of the Wnt signaling required for multiple processes in development, in the adult and in carcinogenesis. We have previously reported that Ror-2 is expressed along the crypt to villus axis in the mouse jejunal epithelia. Furthermore, we have also shown that during the transition of adenoma to colorectal carcinoma, there is epithelial loss of the extracellular calcium sensing receptor, Wnt5a and Dkk-1. Interestingly, in the same tissue micro-array we found a marked increase of Ror-2 expression. While examining the significance of the previous finding, we discovered that overexpressing Ror-2 in colon cancer cell lines that constitutively secreted Dkk-1 resulted in activation of a β-catenin reporter. We then hypothesized that whether Ror-2 interacts with Dkk-1, this interaction should have distinct effects than its known ligand, Wnt5a.
Design: To determine if Dkk-1 and Ror-2 physically interact, we co-transfected several colonic adenocarcinoma cell lines with Dkk-1 and full lenght-Ror-2 or Ror-2 binding domain truncation constructs, and co-immunoprecipitation as well as co-immunofluorescence were performed. To determine whether Dkk1 and Wnt5a functionally interact with Ror2 in a distinct manner, we co-expressed either Dkk-1/Ror2 or Wnt5a/Ror2 in the colonic HT-29 and RKO adenocarcinoma cell lines for 48 hours. We then determine their respective effect on SGLT-1, a downstream target of the homeobox CDX2, at the transcriptional (semi-QRT-PCR; or, SGLT-1 promoter assay assays) and protein (Western Blot) levels.
Results: Co-immunoprecipitation assays showed that intact CRD or Kringle domains of Ror-2 are required for Dkk-1 binding. Furthermore, co-immunofluorescence demonstrated that the physical interaction of Dkk-1 and Ror-2 occurs at the membrane level. Dkk-1/Ror2 stimulation of CDX2 and SGLT1 occurred with an EC_{50} ~ 5 ng/ml. Furthermore, Dkk-1/Ror2 stimulation of CDX2 production required Src. In contrast, Wnt5a/Ror2 stimulation of CDX2 appears faster and required JNK, CK1 and Src.
Conclusions: Dkk-1 physically interacts with Ror2 to signal in a different manner than Wnt5a interacting with Ror2. We speculate that our newly found Dkk-1/Ror2 interaction may account for some of the β-catenin independent effects of Dkk-1.

1686 FBP Knock-Out Leads to a Hematopoietic Maturation Defect.

E Parrilla-Castellar, W Zhou, J Liu, L Tessarollo, D Levens. National Institutes of Health, Bethesda, MD; National Institutes of Health, Frederick, MD.
Background: As a critical regulator of proliferation, growth, differentiation and senescence, the expression of c-Myc is under tight control. A key regulator of c-Myc expression is the FarUpStream Element (FUSE) Binding Protein (FBP). Although the mechanism of FBP-mediated regulation of c-Myc expression has been studied in cell culture, the role of FBP in development has not been studied.
Design: To study FBP function in mice, a 2037 bp fragment encompassing the DNA binding domains KH2, KH3 and part of the KH4 of FBP was deleted. Expression of the knockout allele was not detectable. The phenotype of the FBP knockout was examined.
Results: FBP-deficient mice were embryonic and fetal lethal. Intrauterine death occurred over a broad range of development (E12.5-birth). Mouse embryonic fibroblasts derived from E12.5 embryos showed complete loss of FBP and decreased c-Myc protein expression. Morphologic evaluation of FBP-KO mice at E19.5 showed intrauterine growth delay and ecchymotic discoloration of the skin suggesting a bleeding diathesis. Additionally, histologic examination revealed dysmorphogenesis of the embryonic placenta with increased calcifications. Because c-Myc has been linked to hematopoiesis and placental development in mice, we examined FBP-KO hematopoietic precursors from E13.5 fetal livers. Flow cytometry showed an excess of CD48-/CD150+ stem cells (10.65%) compared to wild type (P<0.001) (2.70%) and a deficit of Tert119-positive erythroid precursors indicating a maturation defect.
Conclusions: FBP plays a critical role in vertebrate development due at least in part to its role in hematopoiesis. The broad range in embryonic demise is consistent with the notion that FBP may serve to regulate stochastic variation in c-Myc expression.

1687 Ploidy and Gender in Cancer Survival.

I Petersen, S Schulze. Jena University Hospital, Jena, Germany.
Background: Ploidy is related to the chromosome complement or the DNA content of cells with aneuploidy being defined as numerical chromosome aberrations or DNA content deviations from the normal state. Ploidy and gender were both related to cancer survival. We aimed to characterize these phenomena in a wide spectrum of neoplasms and to look for potential correlations. In addition we were interested in the ploidy level of different tumor types, in particular the state of near-triploidy.
Design: To characterize the influence of gender a literature search was performed for 27 tumor types. All entities were categorized by the strength of evidence based on the number of studies reporting differences in survival between men and women. In addition, the Mitelman database of chromosomal alterations was evaluated for the major tumor types occurring in both women and men. Numerical gonosome alterations were documented and mean chromosome numbers were converted into histograms to provide insight into the ploidy level of 37 cancer types.
Results: In total, 36.859 karyograms from the Mitelman database were analyzed. Numerical gonosome alterations were more frequent in males than females suggesting a potential link with gender differences in survival. Near-triploidy was a common phenomenon in many, but not all tumor types suggesting that it represents a metastable condition of the cancer genome. It was not related to gender differences in survival. However, the extent of triploidy and aneuploidy was associated with poor prognosis in carcinomas. There was no single case in the Mitelman database with normal chromosome number (n=46) that did not carry at least one structural or numerical aberration.
Conclusions: The data highlights the importance of chromosomal changes in tumor formation and progression. Near-triploidy is a common phenomenon and potentially linked to poor prognosis. Published data indicate that tripolar mitoses are related to triploidy and may thus be used as a surrogate marker for this ploidy state. In addition, triploidy/tripolar mitosis may be useful for differential diagnosis since it is virtually absent in some tumor types while frequent in others. Genomic imbalance of the sex chromosomes is potentially related to gender differences in survival.

1688 Alternative Lengthening of Telomeres in Human Carcinoma Subtypes.

A Proctor Subhawong, C Heaphy, S-M Hong, M Goggins, E Montgomery, E Gabrielson, G Netto, W Westra, P Argani, C Iacobuzio-Donahue, I-M Shih, M Torbenson, A Meeker. The Johns Hopkins University School of Medicine, Baltimore, MD.
Background: Approximately 10-15% of human cancers do not show evidence of telomerase activity, and a subset of these maintain telomere lengths by a genetic recombination-based mechanism termed alternative lengthening of telomeres (ALT). The ALT phenotype, relatively common in certain sarcomas and germ cell tumors, has only rarely been reported in carcinomas. It has been suggested that telomerase expression is more stringently suppressed in mesenchymal tissues, potentially explaining the higher frequency of ALT in sarcomas; however, the prevalence of ALT has not been

thoroughly assessed in carcinomas. Our lab recently reported ALT in a small subset of breast carcinomas; it has also been detected in some adrenal cortical carcinomas. The purpose of this study was to systematically investigate the frequency of ALT in epithelial tumors.
Design: We analyzed tissue microarrays (TMA) of carcinomas of breast (n= 116), salivary gland (n=31), lung (n=197), liver (n=91), kidney (n=114), ovarian serous (n=46), stomach (n=89), colon (n=104), small intestine (n=195), pancreas (n=432), and esophagus (n=88). The arrays included an assortment of primary and metastatic tumors. A sarcoma TMA (n=36) was used as a positive control. Telomere lengths were directly assessed using fluorescence in situ hybridization (FISH) with combined promyelocytic leukemia (PML) protein immunofluorescence.
Results: The ALT phenotype was identified in 7 of 91 primary liver carcinomas and 2 of 114 conventional renal cell carcinomas (1 primary, 1 metastatic). A fourth ALT-positive case was identified in a primary breast carcinoma, in addition to the 3 previously reported from our lab. In summary, 1,503 total carcinomas were analyzed yielding 13 cases of ALT (overall frequency = 0.86%).
Conclusions: This is the first observation of the ALT phenotype in liver and kidney tumors. ALT is very rare in carcinomas overall; observation in our study was restricted to 3 tumor types (breast, liver, and kidney). The telomere maintenance mechanism confers a poor prognosis in some cancers; further studies are needed to assess the prognostic significance and unique biology of carcinomas that express ALT. As cancers using the ALT pathway are predicted to be resistant to therapies based on telomerase inhibition, these results may have therapeutic consequences.

1689 Expression and Function of Erythropoietin Receptor (EpoR) Variant Forms in Human Breast Cancer.

Z Rakosy, G Paragh, G Acs. Moffitt Cancer Center, Tampa, FL.
Background: Recombinant human erythropoietin (rHuEpo) is widely used in the management of cancer and therapy related anemia in patients with breast cancer. Although rHuEpo is effective in correcting anemia and improving quality of life, recent clinical trials suggested a potential adverse effect on patient outcome. Currently the role of EpoR and the effect of exogenous Epo in breast cancer is unclear. We have recently identified variant EpoR forms lacking the N-terminal ligand-binding domain in ovarian carcinoma cells. In this study we investigated the expression and function of EpoR and its variant forms in breast cancer cell lines and clinical samples of human breast cancer.
Design: To identify full length and variant EpoR mRNA forms we used a SMART RACE PCR assay. DNA purified from individual bands was subjected to sequence analysis. To identify variant EpoR forms in human breast cancers, 180 macrodissected formalin-fixed paraffin-embedded invasive breast carcinomas were used for quantitative RT-PCR analysis applying EpoR exon 2-3 and 6-7 specific Taqman assays. The activation of EpoR signaling mechisms, and in vitro and in vivo tumor growth of the cells were examined in MDA-MB-436 cells stably transfected with full length, variant or both EpoR forms.
Results: Using quantitative RT-PCR we found that mRNA regions coding for the extracellular domain of EpoR were expressed at significantly lower levels compared to the C-terminal region in breast cancer cells. Among 180 archived human breast cancer samples, 28.9% of tumors showed more than 10-fold difference between the expression levels of the C and N-terminal regions of EpoR. Using SMART RACE PCR, in breast cancer cells and human breast cancer samples we identified a common 900 bp length EpoR sequence found in most samples. Sequence analysis showed that this band contains only exons 5-8 of EpoR, with exons 1-4, coding for the N-terminal extracellular ligand binding domain of the receptor, completely missing. Breast cancer cells expressing both full length and variant EpoR forms showed increased EpoR signaling and increased tumor growth both in vitro and in vivo in a tumor xenograft model.
Conclusions: Our results indicate that variant forms of EpoR lacking the ligand binding domain are present in human breast cancers and appear to be biologically active, affecting EpoR signaling and tumor growth. Characterization of EpoR variant forms will lead to our better understanding of the mechanisms and role of EpoR signaling in breast cancer and may provide means for the selection of patients for safe, individualized supportive treatment by rHuEpo.

1690 The Pathological Spectrum of Neutrophil DNA NET Formation.

D Salina, FH Pilsczek, C Fahey, FHY Green, P Kubes, M Kelly. University of Calgary, AB, Canada.
Background: Neutrophil extracellular traps (NETs) are webs of DNA covered with antimicrobial molecules that constitute a newly described killing mechanism in innate immune defense (Brinkmann et. Al, ***Science*** 2004). Neutrophils respond to *Staphylococcus aureus* and other bacteria via a novel process of NET formation. NET formation has recently shown to be a major player in the pathogenesis of lupus nephritis, small vessel vasculitis, and cystic fibrosis (Marcos et al, Nature Med. 2010). The use of live cell light microscopy and transmission electron microscopy has identified morphological changes of the nuclear envelope integrity during invitro NET formation (submitted J.Immunol.). We include a retrospective observational study to identify the spectrum of NET formation in various human diseases.
Design: Neutrophils were collected from humans, activated with S. *aureus* and then fixed at various time points. The images obtained from the electron microscope were correlated with live cell imaging. Different cases of purulent inflammation also form NETs, including suppurative appendicitis. We detect NETs using immunoflourescence and immunohistochemistry using antibodies against citrullinated histones. Electron microscopy was performed to compare the ultrastructure to the invitro formed NETs.
Results: NET formation in-vitro is a highly complex process. Initially, the lumen of both the nuclear envelope filled with nuclear chromatin strands. Numerous chromatin containing vesicles budded from the nuclear envelope into the cytoplasm. Eventually nuclear envelope breakdown occurred in a similar fashion to previously published studies (Salina et al, ***Cell*** 2002, Vol.108). The vesicles are exocytosed into the extracellular space where they release their contents. Extracellular NETs form fibrillary structures made up of chromatin strands admixed other proteins from granules.This process of NET formation in purulent appendicitis has identical morphological changes, with numerous extracellular DNA containing vesicles and NETs. We are currently trying to analyze a broad spectrum of various human diseases that also involve formations of these NETs.
Conclusions: The neutrophil nucleus is a highly malleable structure with the capability to undergo drastic changes in nuclear morphology when activated by bacteria. Neutrophils form DNA NETs from a highly complex process which includes nuclear envelope breakdown and exocytosis of DNA containing vesicles. This mechanism is an important part of our inflammatory response to acute infection.

1691 Validation Study for Use of Digital Microscopy for Primary Diagnosis in General Pathology.

L Schoenfield, R Slaw, S Mackie, S Crisostomo, P Suydam, T Bauer. Cleveland Clinic, OH.
Background: Telepathology is a rapidly developing field offering pathologists the ability to remotely review and share diagnostic images.
Design: The aim of the study was to examine real time digital pathology for primary diagnosis. 150 cases from a general pathology practice were examined by one pathologist (LS) using the Aperio whole slide imaging system. Slides were scanned and collated with electronic demographics, working draft and anatomic pathology history. A diagnosis was dictated at the time of digital review but sign-out was delayed until review of derivative glass slides. The glass slides were subsequently reviewed (less than 12 hours following review of the digital images) and time spent, diagnosis, discrepancies if any, and comments recorded.
Results: 150 cases were examined (39 GYN, 37 GI, 33 ocular, 11 GU, 14 soft tissue, 9 ENT, 3 bone, 3 IHC, 1 skin). There were 139 benign lesions, 18 of which were inflammatory, 4 dysplasias, and 7 malignancies. Additional time spent for digital review was: 112 cases 0-1 minute, 24 cases 2-3 min. and 8 cases 4-12 min. In 6 cases digital analysis time was less by 2-5 min. Confidence in diagnosis from the digital image was high (score of 1) in 146 of the 150 cases. The 4 problematic cases were due to inability to focus on a thick fragment (but same on the glass slide), inability to refract gout crystals, and difficulty in seeing possible/few microorganisms. Discrepancies were considered minor and occurred in 5 cases: change in diagnosis from hyperplastic polyp to sessile serrated polyp in 2 cases, addition of focal active inflammation in 2 cases (tonsils and gastric mucosa) and finding of a focus suspicious (but not diagnostic) of cervical dysplasia in an ECC (digitally called negative).
Conclusions: Digital pathology offers advantages over conventional optical microscopy including expedient remote analysis, retrieval of data, and consultations without transporting slides. This reviewer also found that the digital images were subjectively better for diagnostic analysis. Concordance was excellent, and the minor discrepancies noted can be eliminated with practice and experience. Unresolved issues include time spent scanning the images, image storage, ability to focus through thick or folded tissue, refraction, and also licensing and legal issues.

1692 Raman Molecular Imaging Differentiates Epithelioid Mesothelioma from Metastatic-to-Pleura Bronchogenic Adenocarcinoma.

AM Schreiner, JS Maier, AJ Drauch, S Paul. Weill Cornell Medical College, New York, NY; ChemImage Corporation, Pittsburgh, PA.
Background: Raman molecular imaging (RMI), based on Raman spectroscopy, allows for reagentless, nondestructive molecular analysis of biologic samples. RMI produces a digital image with contrast resulting from laser light scatter. Epithelioid mesothelioma (EM) and metastatic-to-pleura bronchogenic adenocarcinoma (MAC) have similar morphology by light microscopy. We describe a pilot study using RMI to differentiate EM from MAC.
Design: Five cases of EM (3 women, 2 men; mean age 66 years) and 5 cases of MAC (2 women, 3 men; mean age 62 years) were selected based on classic clinicopathologic findings. Unstained thin sections from formalin-fixed paraffin-embedded tissue were prepared on aluminum-coated slides. RMI experiments were acquired on each sample using a Falcon II™ Raman microscope. Principal components analysis (PCA) was employed to reduce the data to a set of principal components (PCs) and to determine differences between the sample groups.
Results: Comparing the mean Raman spectra of EM and MAC demonstrated the greatest variance between 1200 and 1410 cm^{-1}. Using this range, a PCA scatter plot showed a significant difference along PC2.

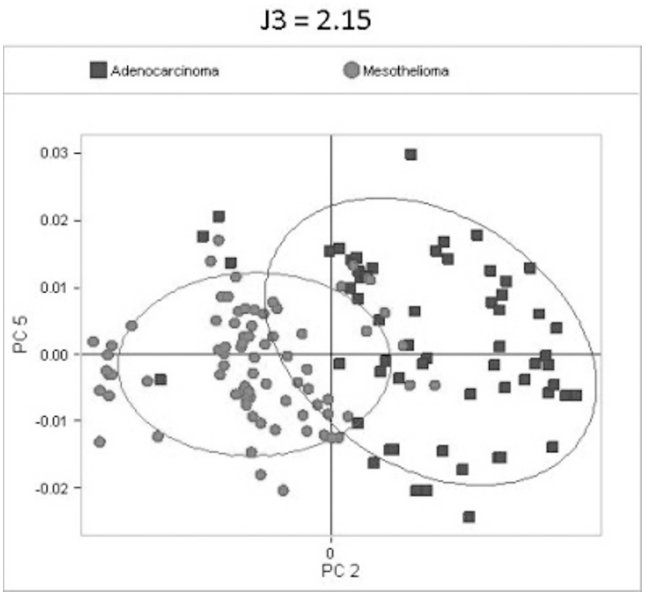

A leave-one-out cross validation for classification based on the weight in PC2 from a given case was done to estimate classification performance of RMI. Nine of 10 samples classified correctly, a sensitivity of 100% and a specificity of 80% for identifying MAC. Digital stains created with RMI data were mapped to corresponding H&E-stained images.

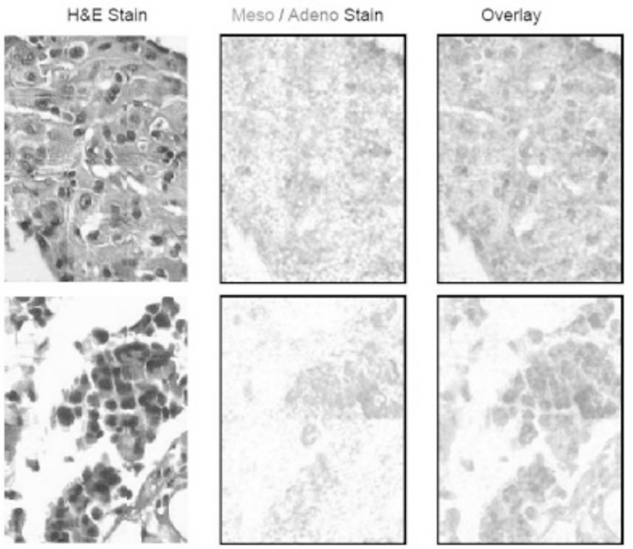

Conclusions: This pilot study shows a statistically significant difference in Raman scattering signatures between EM and MAC. A larger case study is warranted to validate our observations. RMI is a potentially useful diagnostic methodology and may be applicable in other organ systems.

1693 Whole Transcriptome Profiling of Pure Cell Populations Isolated from Minute Prostate Needle Core Biopsies.

J Sweet, N Stickle, C Virtanen, L Qi, S Done, T Brown, K Hersey, N Fleshner, N Winegarden. University Health Network, Toronto, ON, Canada; Mt.Sinai Hospital, Toronto, ON, Canada.

Background: Prostate cancer (PCa) research has focused on the malignant prostate epithelium. However, increasing evidence has shifted focus to the tumor stroma as key in the growth and metastasis of PCa. For a more complete understanding of the role of both epithelium and stroma in the development and progression of PCa, it is necessary to obtain pure cell populations through techniques such as laser capture microdissection (LCM). Typically however, in order to study cells at the whole transcriptome level, tens to hundreds of thousands of cells must be isolated to provide sufficient material. When utilising needle core biopsies, the ability to obtain sufficient material is limited and often mulitple cores are necessary leading to increased heterogeneity of the cell population. We present a novel method of RNA amplification that requires very few (less than 1000) cells and no RNA purification, yet allows robust full transcriptome profiling.

Design: Needle core biopsies were obtained intraoperatively at the time of prostatectomy to obtain tumor and non-tumorous samples from 5 cases. The control group consisted of 5 cases of benign prostate tissue taken in an identical manner at cystoprostatectomy for bladder cancer with no prostate cancer. The tissue was snap frozen in OCT medium. Sections were obtained in RNAse free conditions and stained with hematoxylin. LCM was performed using the Arcturus Pixell LCM system to separately collect epithelial cells and stroma for a total of 30 samples. For each sample, cells were lysed and mRNA was reverse transcribed into cDNA. Using a unique method of multi-stage PCR amplification, double-stranded product was produced in such a way as to maintain transcript abundance relationships. DNA product was dye labeled and hybridized to Agilent 44k whole genome microarrays.

Results: Data was filtered to show only probes that were in the upper 80th percentile of the distribution of intensities in 75% of any of the 1 of 6 above categories. Using a two-way ANOVA we were able to find 571 genes that differed in expression across all 3 tissue types between stroma and epithelium.

Conclusions: The profiling results reveal epithelial and stromal specific gene signatures that may be useful in revealing the complex nature of the interaction between these two tissue components in prostate cancer. In addition, the technique described here will have value for analysis of any tissue samples for which only small amounts are obtainable.

1694 Role of Meis1 in the Transcription of Mitochondrial Genes.

M Tomoeda, Y-F Jin, M Yuki, C Kubo, H Yoshizawa, Y Nishizawa, Y Tomita. Kobe International College, Hyogo, Japan; Osaka Medical Center for Cancer and Cardiovascular Diseases, Japan.

Background: Our previous studies showed that Hox cofactors (Pre B cell transcription factors: PBXs and Myeloid ectopic viral integration sites: MEISs) as important transcription factor of *Valosin-containing protein* (*VCP*). To elucidate difference of function among PBXs and MEISs as transcription factors, cDNA microarray analysis was performed using siRNA transfected pancreatic cancer cell line Panc-1. The result showed down-regulation with *MEIS1* siRNA-transfection and upregulation with *PBX1*, and *PBX2*-transfection of mitochondrial genes.

Design: Luciferase reporter constructs containing serially deleted transcription initiation site of mtDNA were transfected into Panc-1. The deletion and mutation at the binding motifs of MEIS1 was introduced. Chromatin immunoprecipitation assay was carried out to find the binding of MEIS1 to the transcription initiation site of mtDNA. MEIS1 siRNA was transiently transfected to Panc1, and expression of mitochondrial genes was analyzed by cDNA microarray and quantitative PCR. Deletion of mitochondrial membrane potential was observed by fluorescence microscopic examination with JC-1.

Results: The deletion and mutation at the binding motif of MEIS1 reduced the luciferase activity, indicating that the MEIS1 motif mediated the transactivation of mitochondrial gene. Chromatin immunoprecipitation assay showed the binding of MEIS1 to the transcription initiation site of mtDNA. The knockdown of MEIS1 by siRNA decreased the expression level of mitochondrial genes and mitochondrial membrane potential.

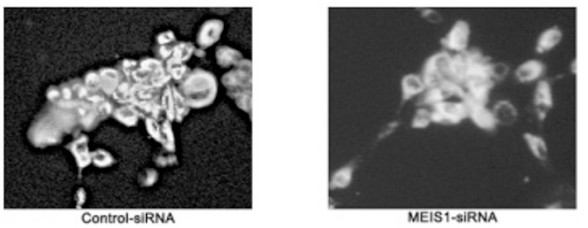

Conclusions: These findings indicate that MEIS1 plays a crucial role in mitochondrial gene expression.

1695 Osteoactivin Expression in Normal Human Tissues, Prostatic Adenocarcinoma and Renal Cell Carcinoma, Clear Cell Type.

GK Uppal, Y Huang, X Zhang, FF Safadi, W Tang, J Khurana. Temple University Hospital, Philadelphia, PA.

Background: Osteoactivin/Glycoprotein nonmetastatic B (GPMNB) is a bone morphogenic transmembrane glycoprotein synthesized by osteoblasts. Increased expression of osteoactivin is associated with osteoblast differentiation and matrix mineralization. Osteoactivin expression has been observed in cell lines of melanomas, meningiomas, hepatocellular carcinoma and is shown to promote metastatic and invasive potential in breast cancer, prostate cancer and gliomas via activation of metalloptroteinases. Exact role of osteoactivin in cancer expression and aggression is not clear at present. The aim of the study was to observe osteoactivin expression some normal human tissues, in malignancies with preferential osteoblastic (prostatic adenocarcinoma) and malignancies with preferentially osteolytic metastasis (Renal Cell Carcinoma, Clear Cell Type). To our knowledge till date there is no study reported in the literature on real human pathological tissues.

Design: Routine Hematoxylin and Eosin and immunohistochemical staining was performed on random sections of fetal bone, mature bone, small intestine, large intestine, breast, placenta and skin tissues, 18 cases of Renal Cell Carcinoma, clear cell type and 18 cases of adenocarcinoma of prostate. The anti-osteoactivin antibody (Human Osteoactivin/GPNMB MAb, R&D Systems) was used for this study.

Results: Osteoactivin staining in random tissue revealed a positive cytoplasmic staining in mature osteoblasts, small intestine epithelium, duct epithelial cells of breast, decidual cells of placenta and basal layer of skin. The staining was negative in colonic epithelium, stromal tissue of breast and chorionic Villi. 4 (22%) cases of renal cell carcinoma were positive for osteoactivin expression out of 18 cases. 5 cases (28%) of adenocarcinoma prostate were positive out of 18 cases.

Conclusions: Small intestinal epithelial cells, basal layer of skin, ductal epithelium of breast and decidual cells are immunoreactive for osteoactivin. There is no difference of

osteoactivin expression between adenocarcinoma, prostate and Renal Cell Carcinoma, Clear Cell type. This is the first study that observed the expression of osteoactivin in actual human pathology tissue samples.

1696 Circadian Dysregulation in Colorectal Cancer: Decreased Nuclear Translocation of Cryptochrome 2.

MA Valasek, RN Van Gelder, SM Dintzis. University of Washington Medical Center, Seattle.

Background: There is growing evidence that circadian rhythms impact development and response to treatment of cancer. Mice lacking critical circadian 'clock genes' have increased rates of tumor development. Cryptochromes are a family of transcriptional repressors which are critical to the core circadian clock mechanism in mammals. Loss of cryptochromes in mice suppresses cancer development in p53 knockout mice. Recent data demonstrate that cryptochrome expression level is a prognostic marker for B-cell lymphoma. The role of cryptochrome expression in solid tumors has not been evaluated to date. In this study, we analyzed the expression of Cryptochrome 2 (Cry 2) by immunohistochemistry in colorectal carcinoma and pre-malignant lesions.

Design: Using human tissue microarrays containing 204 sections, including non-neoplastic, adenomatous and carcinomatous colon and metastatic disease, we determined nuclear expression of p53 and Cry2 by immunohistochemistry. Nuclear expression levels were quantified using the Allred scoring method applied to appropriate cell populations. Microarrays were scored by two independent readers. Significant differences between groups were determined by ANOVA with post-hoc testing.

Results: Nuclear Cry2 staining levels showed significant variation across classes of colon tissue, ranging from near 100% expression in benign colon to 41% expression among lymph node colorectal metastases. Nuclear Cry2 was significantly downregulated when comparing normal tissues with large tubulovillous or villous adenomas, adenocarcinoma at T1-T2 stage, or T3 stage (decreased 39-56%). Cry2 staining was generally inverse to p53 staining except in large adenomas.

Conclusions: Cry2 nuclear expression is decreased in colorectal cancers and large adenomas. This finding suggests that the circadian clock is progressively dysregulated in pre-malignant and malignant lesions of the colon. Further studies will determine if Cryptochrome expression has prognostic significance in colorectal carcinoma.

1697 ABCB5 Is Expressed by Placental Cytotrophoblasts.

ER Volpicelli, Q Zhan, DW Kindelberger, MH Frank, NY Frank, CP Crum, GF Murphy. Brigham and Women's Hospital, Boston, MA; Children's Hospital, Boston, MA.

Background: Transport proteins play important roles in regulating exchange across the placental maternal-fetal interface. P-glycoprotein (P-gp) encoded by the MDR1 gene is one of the best characterized ATP-dependent drug efflux transporters in the placenta. P-gps (specifically ABCB1) expressed on the maternal facing border of syncytiotrophoblast microvilli, participate in the efflux of hydrophobic and cationic agents into the maternal blood, reducing chemical exposure to the fetus. ABCB5 [subfamily B (MDR/TAP)] is a novel human ABC transporter encoded on chromosome 7p15.3. ABCB5 is expressed on the plasma membrane of physiologic human skin progenitor cells and chemoresistant melanoma stem cells; functions as a rhodamine efflux transporter and regulates membrane potential and the resultant propensity for cell fusion. ABCB5 expression in trophoblastic cells (both neoplastic and non-neoplastic) has never been described.

Design: ABCB5 immunohistochemistry was performed (as previously described: *Nature* 451:345-349, 2008) on formalin fixed, paraffin embedded placental tissue from five early pregnancies (< 10 weeks gestational age), 5 term pregnancies, 5 partial moles, and 5 complete moles. Additionally tumor cells from 5 choriocarcinoma, and 5 placental site trophoblastic tumor (PSTT) cases were examined.

Results: Perinuclear and membranous/cytoplasmic ABCB5 staining was observed in villous cytotrophoblasts in 100% (5/5) of first trimester placentas, 0% of term placentas (0/5), 100% of partial moles (5/5) and 100% of complete moles (5/5). Notably, reactivity was discretely restricted to the cytotrophoblast layer, with no staining of overlying syncytiotrophoblast. There was staining in 20% of choriocarcinomas (1/5) and 40% of PSTTs (2/5).

Conclusions: Prior studies have localized expression of MDR-1, ABCB1, within the syncytiotrophoblasts of early placentas. Its function may be protective based on efflux function at the level of cell membranes. Our results show that ABCB5 is preferentially expressed in villous cytotrophoblasts, a stem cell population, which through cell fusion gives rise to syncytiotrophoblasts. Thus, in addition to the coordinated protective efflux function common to ABCB5 and other P-gp transporters at the maternal-fetal interface, ABCB5 may specifically be involved in fusion events inherent in syncytiotrophoblast formation. Studies are presently underway to test this hypothesis both in vitro as well as in the context of human conditions potentially involving defective syncytiotrophoblast formation.

1698 Immunohistochemical Characterization of Pancreatic Adenocarcinomas Arising in Association with Intraductal Papillary Mucinous Neoplasms.

AK Witkiewicz, J Brody, J Kline, CJ Yeo, P McCue, NV Adsay, RH Hruban. Thomas Jefferson University, Philadelphia, PA; Johns Hopkins University, Baltimore, MD; Emory University, Atlanta, GA.

Background: Most pancreatic adenocarcinomas (PAs) arise from pancreatic intraepithelial neoplasia (PanIN) for which molecular and immunohistochemical features have been well characterized. However, less studied are the PAs that arise from another precursor, intraductal papillary mucinous neoplasm (IPMN). In this study we correlated the pathology of 22 PA arising in association withan IPMN with immunohistochemical markers implicated in PA pathogenesis.

Design: The criteria for the inclusion in the study included radiologically and macroscopically visible cystic dilatation of pancreatic duct and presence of well defined papillae on histologic review. Histologic type of IPMN and invasive carcinoma was recorded for all cases. Immunohistochemical labeling for DPC4, p53, p16, Ki67, CDX2, MUC1, MUC2 was preformed on all cases.

Results: Nine IPMNs were intestinal, 6 pancreaticobilliary, 5 gastric and 2 mixed type. All cases showed at least focal high-grade dysplasia (carcinoma *in situ*). Associated PA was colloid in 4 cases, tubular in 16 and tubular with mucinous features in 2 cases. PAs arising from intestinal and gastric IPMNs tend to be better differentiated than those arising from pancreaticobilliary IPMN. MUC2 and CDX2 positivity were seen in the intestinal type IPMN, mucinous PA, and in the tubular carcinomas with mucinous features. DPC4 loss was seen in 4 of 9 tubular PA arising from pancreaticobilliary IPMN and only one arising from intestinal IPMN. Loss of p16 occurred in both tubular and mucinous PA. P53 expression was seen only in tubular PA.

Conclusions: PAs arising from IPMNs have a number of unique and similar molecular features to other precursors. Molecular classification of these lesions may provide valuable prognostic information and reveal potential early targets that may be shared with PanIN precursor lesions.

1699 The Roles of BDNF and SDF-1 Expression Levels and Polymorphisms in the Development of Intraventricular Hemorrhage in the Premature Infant Population.

Y Wu, S Canosa, Q Li, V Glinskii, I Buhimuschi, J Madri. Yale University School of Medicine, New Haven.

Background: Low birth weight preterm infants suffer from perinatal hypoxic-ischemic encephalopathy. Increased BDNF and SDF-1 levels were correlated with the survival /responsiveness of neuron stem cells. The BDNF Val66Met polymorphism was demonstrated in neurological impairments. SDF-1 G801A polymorphism is involved in tumor invasion. These findings have prompted this cord blood study, with a goal to provide novel biomarkers in predicting the risk for severe/persistent neurodevelopmental handicaps.

Design: 1. Cord blood samples were collected from preterm infants with weight <1250 gram, and divided into three groups: intraventricular hemorrhage only (IVH), early-onset sepsis status only (ENOS) and controls without intraventricular hemorrhage or sepsis (NO IVH). 2. ELISA determination of cord blood BDNF. 3. BDNF and SDF-1 polymorphism determination using DNA loci of interest amplification and RFLP analysis.

Results: 1. BDNF level was 113.4 pg/mg in IVH group, significantly less than that of No IVH control group (151.5 pg/mg, $p<0.01$).

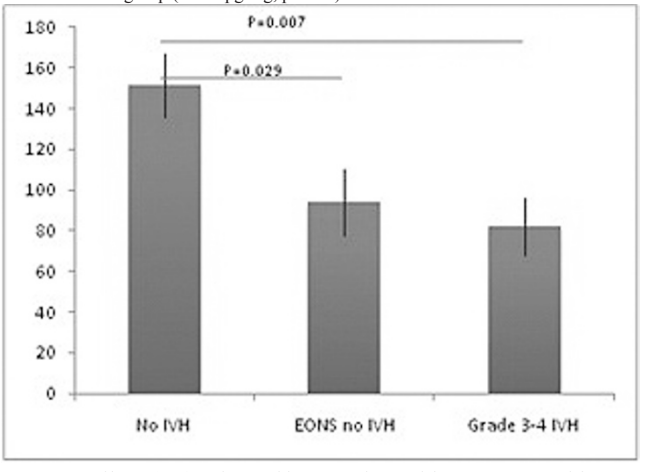

2. BDNF Val/Met (GA) polymorphism was detected in 25% IVH, and in 16% ENOS; while Met/Met (AA) was shown in 12.5% control group. 3. SDF-1 G801A polymorphism was detected in 50% control group, markedly higher than that of IVH group (11%), and EONS group (0%).

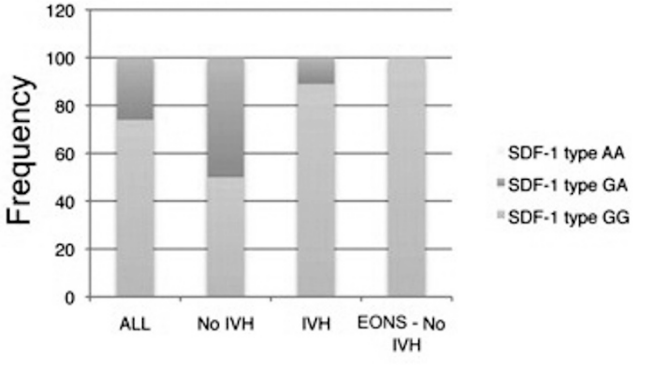

Conclusions: 1. BDNF-1 cord blood level was significantly decreased and Val66Met polymorphism was slightly increased in preterm infants with IVH. 2. SDF-1 G801A polymorphism, a genotype known to promote tumor cell metastasis, was markedly

reduced in preterm infants with IVH or ENOS, which might account for their decreased neurogenesis. The increased incidence of this polymorphism in the control infant brain will presumably foster the stimulation of neurogenesis following hypoxic insult.

1700 High-Throughput Prostate Cancer Gland Segmentation and Classification from Digitized Needle Core Biopsies.

J Xu, R Sparks, A Janowcyzk, JE Tomaszewski, A Madabhushi. Rutgers University, Piscataway, NJ; The Hospital of the University of Pennsylvania, Philadelphia; IIT Bombay, Piscataway, NJ.

Background: CaP grading of histopathology can be divided into two separate tasks: identification of malignant regions and the Gleason grading of the malignant regions. Since manual discrimination of benign and malignant regions by pathologists is a time-consuming process, developing computerized decision support (CDS) systems that can quickly and accurately identify suspicious regions in tissue samples will enable the pathologist to focus their grading efforts on candidate regions, minimizing the time spent on identifying CaP regions. We present a high-throughput system for segmentation and classification of glands in high resolution digitized images, which will allow for rapid and accurate identification of suspicious regions on these samples.

Design: The high-throughput system includes the following three modules: 1) a hierarchical frequency weighted mean shift normalized cut for initial detection of glands; 2) a geodesic active contour model for gland segmentation; and 3) a diffeomorphic based similarity feature extraction and support vector machine for classification of glands as benign or cancerous.

Results: Classification accuracy in distinguishing benign from malignant glands over 23 H & E stained prostate studies when using the automated segmentation scheme was 82.5±9.1%, while the corresponding accuracy with manual segmentation was 82.89±3.97%; no statistically significant differences were identified between the two segmentation schemes. Figure 1 illustrates an example of whole-slide needle core biopsy of the prostate with malignant region delineated in blue. Glands labeled as benign/ normal (black) and malignant (green) by the classifier are displayed.

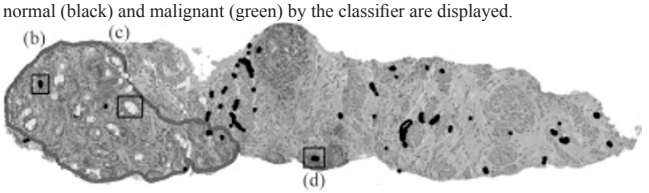

Conclusions: We presented a high-throughput system for rapid and accurate gland segmentation and classification on high resolution digitized whole-slide images of needle core biopsy samples of the prostate. Since our system is able to automatically identify malignant regions with our CDS system, pathologists can save more time on analyzing the malignant regions.

1701 BK Virus-Associated Immune-Mediated Tubulointerstitial Nephritis. Clinicopathologic Characterization.

J Xu, A Abdullatif, G Towns, L Gaber, R Barrios, L Truong. Changhai Hospital, Shanghai, China; Methodist Hospital, Houston, TX.

Background: BK virus-associated immune-mediated tubulointerstitial nephritis (BKV TIN) is a form of chronic tubulointerstitial nephritis chacterized by tubular basemen membrane (TBM) deposition of immunoglulins and complement components, against the background of BKV nephropathy. TBM immune-type electron dense deposits are also noted in several cases. The knowledge on BKV TIN is limited.

Design: All renal transplant biopsies during a 10-year period (2000-2010) were reviewed to identify those with BKV nephropathy alone and those with BKV-TIN. Their clinicopathologic features were compared and contrasted.

Results: Among 730 renal tranplant (Tx) biopsies, 13 biopsies in 9 patients showed BKV+TIN (Group A), and 29 biopsies in 25 patients showed BKV nephropathy only (Group B). TIN with TBM deposition of immunoglobulin G (Ig G) and complement com ponent C3 (C3) was noted in one Tx biopsy without BKV nephropathy. The age and sex in Groups A and B patients were similar (60.3±11.6 vs 60.7±10.6 years; F/M ratio 0.7 vs 0.6). There was no significant difference in the serum creatinine at presentation (2.7±1.8 vs 2.9±1.2mg/dl), the baseline immunosupression, or the blood BKV level by PCR between the two groups. TBM IgG, C3 and C4d for Groups A and B was 100% vs 0%, rare-20% of tubular profiles; 100% vs 31%, few -25% of tubular profiles; and 92 vs 24%, few-30% tubular profiles. TBM electron dense deposits were noted in 2 cases on routine EM. TBM did not show the large T antigen by immunostain in any case of Groups A or B. Chronic tubulointetstitial injury was more severe in Group A (34.0±29.5% vs 27.7±21.4 % of cortical tissue). Multiple biopsies done in four patients in Group A showed that BKV TIN was preceded by BKV nephropathy alone (3 cases), persisted in repeated biopsies (2 cases), or disappeared in repeated biopsy in which BKV nephropathy persisted (1 case).

Conclusions: BKV TIN is probably pathogenetically related to BKV nephropathy since it develops rather frequently (30%) from the background of BKV nephropathy, but only rarely observed in renal Tx biopsy without BKV nephropathy. It seems to be associated with more renal chronic renal injury compared with BKN nephropathy alone. Its evolution is variable with possible persistence of resolution in repeated biopsies.

1702 Elevated Interstitial Pressure Enhances Hypoxia-Induced VEGF Expression Via HIF-1 in Daoy Medulloblastoma Cells.

H Zhong, R Wang, JW Simons. New York University, NY; Emory University, Atlanta.

Background: Tissue hypoxia, increased interstitial pressure and edema are common findings in solid tumor. Hypoxia activates transcription factor HIF-1 and regulates the expression of HIF-1-target genes including the gene that encodes VEGF, a critical factor underlying angiogenesis and interstitial edema. HIF-1α, the dominant subunit of HIF-1, is regulated by oxygen-dependent and –independent ways. We have developed a module to test our hypothesis that increased interstitial pressure enhances hypoxia-induced VEGF expression via HIF-1.

Design: As an alternative to an inflexible hypoxia chamber, we designed a pliable hypoxia chamber to compare cellular responses to three tissue culture environments including conventional CO_2 culture, and hypoxia cultures (1% O_2/5% CO_2/balanced N_2) with or without elevated interstitial pressure. The interior pressure within the chambers were monitored by water-mercury manometers. The pliable hypoxia chamber was 80% filled to mimic hypoxia setting without elevated interstitial pressure. The interior pressure remained at 0 mmHg within 24 hours at 37°C. The inflexible hypoxia chamber was fully filled so as to create an intermediate (40 mmHg) or a high (70 mmHg) interior pressure. After 24-hour at 37°C, the interior pressure was elevated from 40 mmHg to 60 mmHg (intermediate) and from 70 mmHg to 120 mmHg (high), respectively.

Results: The new pliable hypoxia chamber was functional based on our design. Due to transparent and flexible, it could be adjusted to a size which allowed us to periodically record, microscopiclly in real time, the nuclear translocation of GFP-HIF-1α and the endothelial tube formation following continuous exposure to hypoxia. In Daoy cells cultured at 37°C for 24 hours, the intermediate pressure enhanced the hypoxic induction of HIF-1α, HIF-1 transcriptional activity and VEGF production. However, high pressure did not affect HIF-1 but resulted in growth inhibition. Finally, the enhanced signal transduction activity upstream of HIF-1α synthesis was shown in cells under hypoxia with intermediate pressure as compared to those in conventional culture or regular hypoxia culture without elevated interstitial pressure.

Conclusions: Intermediate interstitial pressure augments hypoxia-induced VEGF expression through HIF-1. Increased HIF-1α expression likely involves increased protein synthesis in response to moderate pressure stress. Our results could explain the edematous change seen in pathological conditions such as solid tumors, especially those which are situated within a confined space.

1703 Detection of KRAS Mutation and Loss of Heterozygosity (LOH) in Mucinous Nonneoplastic Cyst of the Pancreas.

B Zhu, SD Finkelstein, Z Chen, X Lin. Northwestern University, Chicago; RedPath Integrated Pathology, Inc, Pittsburgh.

Background: Mucinous nonneoplastic cyst (MNNC) of the pancreas is defined as cysts lined by mucinous epithelium and supported by hypocellular stroma with no communication with the pancreatic ducts. MNNC is a rare and not well recognized entity with unknown histogenesis and etiology. It shares many clinical and radiological features with mucinous cystic neoplasm (MCN) and intraductal papillary mucinous neoplasm (IPMN), particularly the branch type, therefore, creating great diagnostic challenge for cytological evaluation of FNA specimens. To explore a petential role of molecular test in aiding diagnosis and distinguish it from MCN and IPMN, we analyzed KRAS mutation and LOH in MNNC.

Design: 24 surgically resected MNNCs were retrieved. The cystic lining epithelium was microdissected for molecular tests: 1) KRAS mutation (1st exon) (DNA sequencing), and 2) allelic imbalance (LOH) for a panel of 16 polymorphic microsatellite repeat markers targeting tumor suppressor genes and situated at 1p, 3p, 5q, 9p, 10q, 17p, 17q, 18q, 21q, and 22q. Cystic fluid CEA and amylase concentrations were also retrieved.

Results: CEA ranged from 75.2 to 5,488 ng/ml and amylase from 19 to 28,478 U/L. Molecular studies on 15 of 24 cases showed that 4 cases had 1 genomic mutation, 1 with KRAS mutation at 12D (40% of cells), 1 with KRAS mutation at 12R (20% of cells), 1 with LOH at 10q (50% of cells), and 1 with LOH at 17q (60% of cells).

Conclusions: Detection of CEA and amylase levels in cystic fluid is not useful to distinguish MNNC from IPMN and MCN. Molecular study results indicated that 4 of 15 (27%) surgically diagnosed MNNCs acquired 1 low amplitude (< 75% of cells) genomic mutation, 2 K-RAS mutations, 1 LOH at 10q (pTEN) and 1 LOH at 17q (HER2/neu and NF1). Although the genomic mutation rate detected in MNNC is very low, the data indicated that rare MNNC may acquite genetic alteration similar to low grade pancreatic intraepithelial neoplasia (PaIN), fuming the debate of the true nature of these lesions.

1704 Physiologic Replication of Human Disease with Murine Experimental Autoimmune Thyroiditis.

MI Zulfiqar, S Kari, J Flynn, D Snower, Y-C Kong. St John Hospital, Detroit, MI; Wayne State University, Detroit, MI; Providence Hospital, Detroit, MI.

Background: Experimental autoimmune thyroiditis (EAT) is a murine model for Hashimoto's thyroiditis (HT) with characteristics of HT including mononuclear cell infiltration, destruction of thyroid follicles, autoantibody production and T cell proliferative response to thyroid autoantigens. EAT is inducible in genetically susceptible mice by immunization with mouse thyroglobulin (mTg) and adjuvant bacterial lipopolysaccharide (LPS). We devised 3 protocols to better simulate the physiology of human disease. In #1, we replaced LPS with recombinant interleukin (rIL)-1β, a cytokine induced by LPS. In #2, we modulated the immune system by depleting regulatory T cells (Tregs), while reducing the LPS dose. In #3, we injected mTg without adjuvant to mimic fluctuating thyroglobulin levels in the circulation.

Design: #1: EAT-susceptible CBA/J mice (8-12 wks) were injected with 40 μg mTg followed 3 hrs later by 10,000 IU rIL-1β (days 0, 7). Sera were obtained on day 14 and thyroids were processed on day 28. **#2**: Mice were depleted of Tregs by injection of CD25 mAb (days -11, -7). Mice were injected with 40 μg mTg followed 3 hrs later by 0.5 μg LPS (day 7), and mTg only (days 14, 21). **#3**: Tregs were depleted by CD25 mAb treatment (days -14, -10). Mice were injected with 16 doses of 40 μg mTg without adjuvant from days 0 to 24 (4X/week). Thyroids and sera were obtained on day 35. All thyroids were examined for cellular infiltration and follicular destruction. Splenocytes were cultured with mTg, and proliferation was assessed by [^{3}H]thymidine uptake. Anti-mTg levels were quantitated by ELISA.
Results: #1: Moderate thyroiditis, T cell proliferation and anti-mTg levels were observed in all mice treated with rIL-1β. **#2:** Treg-depleted mice had higher thyroiditis incidence and severity, increased T cell proliferation and anti-mTg levels, compared to controls. **#3:** Compared to mice given repeated mTg doses only, Treg depletion led to greater thyroiditis incidence and severity, and higher anti-mTg levels.
Conclusions: EAT can be induced in susceptible mice by treatment with mTg and rIL-1β or reduced LPS. The incidence and severity increase with Treg depletion. When repeated mTg doses without adjuvant followed Treg depletion, EAT incidence and severity are also augmented. These protocols will aid the study of consequences of immunotherapy in susceptible patients or those with pre-existing autoimmune thyroid disease. (Supported by St. John Hosp.)

Pediatrics

1705 Morphoproteomics Provides Further Insight into the Biology of Metastatic Osteosarcoma and Identifies Potential Therapeutic Targets.

S Alexandrescu, P Anderson, J Buryanek, RE Brown. University of Texas- Medical School, Houston; MD Anderson Cancer Center, Houston, TX.
Background: Metastasis in osteosarcoma decreases the survival to 10-25%. Establishing a targeted therapeutic protocol for these patients is challenging, because of genetic instability. However, these tumors have common biologic components that might be targets for therapy (expression of c-Met, TRAIL (DR4), and activation of insulin-like growth factor-1 receptor (IGF1R) signaling pathway).
Design: Three consulting pathologists examined tissue from four MD Anderson Cancer Center patients (age range 11-16) with multiple sites of metastatic osteosarcoma unresponsive to treatment. A morphoproteomic analysis of signaling pathways, cell cycle analytes, antiapoptotic/tumorigenic/angiogenic/chemoresistance factors, proapoptotic proteins and stem cell markers was performed.
Results: We observed: variable activation of ras/Raf kinase/extracellular signal regulated-kinase (ERK) pathway, evident by nuclear translocation of p-ERK1/2 (Thr202/Tyr204) in a majority of the tumor cells; activation of the mammalian target of rapamycin (mTOR) pathway in many tumor cells with p-mTOR(Ser 2448) in both cytoplasmic and nuclear compartments (consistent with variable mTORC1 and mTORC2 activation); brisk cell cycle progression;expression of tumorigenic proteins, heat shock protein (Hsp)90, p-p38MAPK (Thr 180/Tyr182)and fatty acid synthase (FAS); proapoptotic TRAIL-DR4 expression; and a CD133 and nestin stem cell immunophenotype. EGFRvIII/wild type, HER-2 and VEGF-A were absent or weakly expressed in a minority of cells.
Conclusions: This consultative study provides an explanation for the limited efficacy of some of the agents used in these patients (bevacizumab, rapamycin, anti-EGFR antibody), and suggests new targeted therapies.Sorafenib and aminobisphosphonates act to downregulate the ras/Raf kinase/ERK pathway. Metformin inhibits IGF-1R signaling pathway at the level of IRS-1, induces TRAIL-mediated apoptosis in osteosarcoma and contributes to cell cycle arrest. It also inhibits fatty acid synthase, representing a convenient substitute for c-MET inhibitor. Doxorubicin sensitizes osteosarcoma cells, but not normal bone cells to Apo2L/TRAIL-induced apoptosis and targets mitotically active tumor. Melatonin inhibits cell cycle progression and augments chemotherapy while minimizing toxic side effects.

1706 Metformin Induces Cell Death in a Human Neuroblastoma Cell Line through Affecting Multiple Survival Pathways.

H Chai, P Weerasinghe, RE Brown. University of Texas- Medical School, Houston.
Background: Neuroblastoma is the most common extracranial solid cancer in childhood. Its tumorigenicity is enhanced by the expression of survival pathways such as Akt and signal transducer and activator of transcription (STAT)3 as well as an inappropriate level of mammalian target of rapamycin (mTOR) activity. Metformin is one of the most widely used diabetes drugs. It has shown inhibiting effects on mTOR, which may prevent the growth of cancer cells. In this study, we will examine the efficacy of metformin on a human neuroblastoma cell line and also investigate its possible mechanisms.
Design: A neuroblastoma cell line, SK-N-AS, was purchased from ATCC. After reaching 50-60% confluence, cells were treated with various concentrations of metformin (0, 1, 5, 10, 20, 40 mM) for different period of times (0, 30 min, 2, 6, 24, 48 and 72 hours). The cell viability was determined by MTT colorimetric assay. The apoptotic responses were measured with TUNEL assay. Phosphorylation of Akt1/2/3 (p-Akt1/2/3 [Thr308]), AMP-activated protein kinase alpha1 subunit (p-AMPKa1 [Thr172]), p42 MAP Kinase (p-ERK2), STAT3 (p-STAT3 [Ser727]), and mTOR (p-mTOR [S2448]) and total mTOR (mTOR [7C10]) protein expression levels were determined with Western blot assay.
Results: As early as 6 hours post-treatment, cell viability was significantly decreased at 10 mM concentration. In 24 and 48 hours treatment groups, metformin at 5 mM and above concentrations significant decreased cell viability. TUNEL assay showed similar results. Western blots showed a decrease of p-Akt2 and p-STAT3 expression levels in metformin treatment groups. An increase of p-ERK2, p-AMPKa1 was also observed. Total mTOR levels were slight increased while the phosphorylation at S2448 site was significantly decreased.
Conclusions: Our results indicate that metformin significantly decreased cell viability and increased cell death in a human neuroblastoma cell line in association with down-regulation of p-Akt, p-STAT3 and p-mTOR survival pathways. These data suggested a potential clinical application of metformin in the treatment of neuroblastoma cases with constitutive activation of Akt, STAT3 and mTOR.

1707 β-Catenin and Novel Associated Proteins in Nasopharyngeal Angiofibromas.

SL Cook, RD LeGallo, SE Mills, EB Stelow. University of Virginia, Charlottesville.
Background: Nasopharyngeal angiofibromas occur at an increased frequency in patients with familial adenomatous polyposis. Furthermore, a majority of sporadic nasopharyngeal angiofibromas has been shown to have nuclear accumulation of β-catenin and have mutations in the β-catenin gene. These results suggest that the Wnt-signaling pathway is important in the pathogenesis of both sporadic and syndrome-associated tumors. End-binding protein 1 (EB1) is an adenomatous polyposis coli (APC)-binding protein which associates with growing ends of microtubules and has been reported to be overexpressed in some carcinomas. Cyclin D1 is a transcriptional target of β-catenin which promotes cell cycle progression. While WT1 functions in transcription regulation, it is now speculated that it also plays a role as a tumor suppressor of the Wnt-signaling pathway. Here, we examine the expression patterns of β-catenin, EB1, cyclin D1, and WT1 in a series of nasopharyngeal angiofibromas.
Design: The study examined 14 nasopharyngeal angiofibromas resected from 14 males ranging in age from 10 to 23 years and found within the surgical pathology files of a single institution. Immunohistochemistry was performed for β-catenin, EB1, cyclin D1, and WT1. Staining pattern and characteristics and the percentage of cells staining were recorded.
Results: All fourteen nasopharyngeal angiofibromas showed prominent nuclear accumulation of β-catenin. In addition, 13 of 13 showed strong, granular cytoplasmic accumulation of EB1. Cyclin D1 showed nuclear staining in a minority of cells (<10% of cells) in 9 of 14 cases. All fourteen tumors showed cytoplasmic staining with WT1. In 7 of 14 (50%) of cases, cytoplasmic WT1 was present in 20 to 50% of cells, while the remaining 7 cases had staining in 70 to 90% of cells.
Conclusions: We confirm the strong and diffuse nuclear accumulation of β-catenin in nasopharyngeal angiofibromas previously noted by others. Cyclin D1 staining supports the functional status of the activated β-catenin. Interestingly, the expression of the novel protein EB1 suggests a role for APC in these tumors. Also, the expression of WT1 in these tumors known to have β-catenin accumulation provides further evidence of its role as a potential tumor suppressor of the Wnt-signaling pathway. Aside from providing information regarding the pathobiology of these tumors, these results also suggest a possible use for these immunostains in the diagnosis of these tumors.

1708 Intratubular Germ Cell Neoplasia, Unclassified Type (IGCNU), in Prepubertal, Cryptorchid Testes: A 20 Year Experience at a Major Pediatric Hospital.

R Fan, TM Ulbright. Indiana University, Indianapolis.
Background: Maldescended testes frequently come to the attention of pathologists, especially in pediatric hospitals. It remains controversial if prepubertal testes develop IGCNU. We therefore reviewed our experience over a 20-year interval with maldescended, prepubertal testes that carried a diagnosis of IGCNU.
Design: With approval of the Institutional Review Board, we performed several searches in our computerized pathology database from January 1990 to December 2009 to identify all testicular and paratesticular lesions. Next we examined all cases carrying a diagnosis of IGCNU. All were in maldescended testes.
Results: Of 883 testicular and paratesticular specimens, 276 represented atrophy/cryptorchidism (236) or intersex disorders (40). Among these 276 specimens, 6 from 5 patients with cryptorchidism carried a diagnosis of atypical intratubular germ cells. Three patients had a known intersex disorder and, on review, the specimens met the morphological and immunohistochemical criteria for IGCNU. Review of the remaining 3 specimens from 2 patients, who lacked an established diagnosis of an intersex disorder, verified that the atypical germ cells in 1 case lacked the features of IGCNU but showed nuclear enlargement with hyperchromasia and frequent central position within the tubules; these cells did express fetal germ cell markers (OCT3/4, placental alkaline phosphatase, CD117) also expressed in IGCNU and likely reflect delayed germ cell maturation, as has been described in the gonads of patients with undervirilization syndromes. The last patient, who was not known to have an intersex disorder, had a right duplex dysplastic kidney with both upper and lower pole obstruction and bilateral undescended testes. Review of his testicular specimens obtained at 9 weeks and 4 months, showed dysgenetic features, with ovarian type stroma and malformed tubules as well as IGCNU. We therefore consider him to have a previously undiagnosed intersex disorder, a conclusion also supported by the surgeon's intraoperative impression. We therefore did not identify a bona fide case of IGCNU in prepubertal maldescended testes outside of a known intersex disorder or with findings highly suggestive of one.
Conclusions: Based on our experience it is questionable if legitimate examples of IGCNU occur in prepubertal testes apart from an intersex disorder. Careful morphological and immunohistochemical evaluation and correlation with clinical findings are essential in the examination of prepubertal cryptorchid testes to avoid overdiagnosing IGCNU.